Chapter Four
FINITE ELEMENT ANALYSIS

4.1 INTRODUCTION

A finite element analysis was performed with the primary objectives of explaining the various modes of failure observed in the experimental program and extend the results of the test program through a parametric study (Hoffmann 1997). An elasto-plastic finite element parametric analysis was performed to study the behavior of various dent types (restrained and unrestrained) using a three dimensional finite element model in **ABAQUS** v5.5. Dent and pipe parameters are investigated. Dent parameters include dent type, dent depth, and dent restraint. Pipe parameters include diameter, thickness, pipe grade, longitudinal stress, and pipe support. The results from the models include displacement, stress, and strain data. The displacement data is used to study the rebound behavior of various unrestrained dents. The stress data is used to determine possible failure locations and corresponding stress ranges. The displacement and strain data is used to estimate a damage term to reduce a dent's fatigue life provided a conventional fatigue life approach is used to determine the dent's life.

4.2 PARAMETERS

4.2.1 Dent Parameters

A variety of dent parameters were studied by finite element analysis to investigate the behavior of *damaged* pipelines. While the acceptance criteria of dents in pipelines is currently based on dent depth (d), the influence of other parameters in conjunction with dent depth was studied. The dent parameters can be classified by dent depth, dent type, and dent restraint. The dent type includes terms based on geometry, such as the length, width, and orientation of the indenter.

The dent depth was varied based on the ratio of dent depth to pipe diameter (D). The diameters of the pipes investigated ranged from 12 in. to 48 in. The dent depth ratio (d/D) was varied from five percent to fifteen percent by 2.5 percent increments. This gives five depths that are considered to range from shallow to deep. The depths represent the initial dent depth prior to pressurization and indenter removal. While this measure of dent depth is not recordable in the field for unrestrained dents due to elastic rebound, it does provide a constant baseline for comparative reasons. The initial dent depth was also used in the experimental program. Depths higher than fifteen percent were not studied due to model divergence and the lack in confidence of the results. The indenter force required was recorded for the different dent depths. The additional force required to form a deeper dent can result in the puncturing of the pipe wall or severe contact plasticity which requires immediate repair. The dent depths modeled for different pipe sizes is given in Table 4-1.

Table 4-1: Dent depth modeled in finite element parametric study (in.).

Diameter	Initial d/D (%)				
(in.)	5	7.5	10	12.5	15
12	0.60	0.90	1.20	1.50	1.80
18	0.90	1.35	1.80	2.25	2.70
24	1.20	1.80	2.40	3.00	3.60
30	1.50	2.25	3.00	3.60	4.50
36	1.80	2.70	3.60	4.50	5.40
48	2.40	3.60	4.80	6.00	7.20

The dent type parameter was studied by using different indenter types. Examples of the indenters modeled are shown in Fig. 4-1 along with their dimensions. The primary type of indenter used is cylindrical in shape with rounded ends. The overall length was varied between 2.0 and 12.0 inches. This allowed modeling of the indenters used in the experimental program as well as variation of these indenters. For example, a 2 in. long indenter modeled the 2 in. backhoe

tooth (dent Type BH). Dent Type G was not evaluated experimentally, but is similar to Type A, which was evaluated experimentally, but is 12 in. long instead of 6 in. Spherical indenters (Type S1 and S8) were used in the investigation of rock dents. Indenter Type P represents the flat plate used in the AGA experimental program. The indenters were modeled as being fully rigid for the investigation of unrestrained dent behavior. Consequently, all deformation, both elastic and plastic, occurred in the pipe section under investigation. A *summary* of the indenter types investigated are given in Table 4-2.

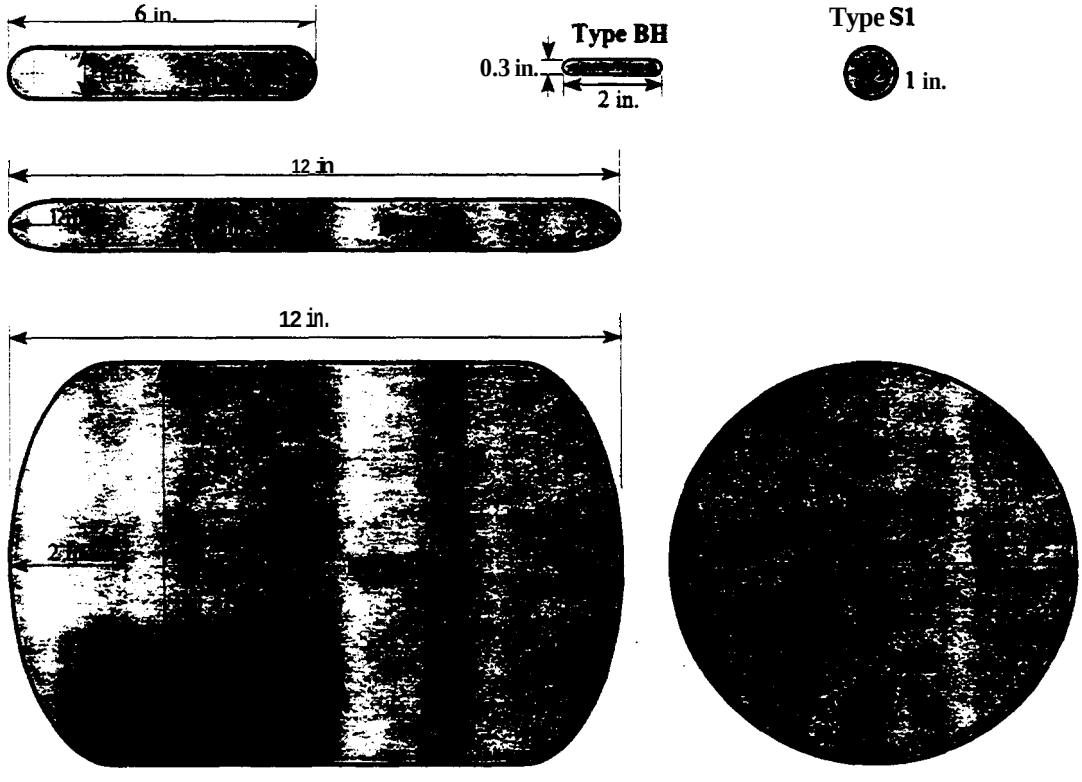

Figure 4-1: Indenter shapes and designations used in the finite element analysis.

Table 4-2: Summary of indenter types used in the finite element analysis.

Indenter Type	Description
A	6 in. cylindrical dent with 1 in. diameter
BH	2 in. backhoe tooth
G	12 in. cylindrical dent with 1 in. diameter
H	12 in. cylindrical dent with 8 in. diameter
S1	sphere with 1 in. diameter
S8	sphere with 8 in. diameter
P	24 in. square plate

The orientation of the indenter, with respect to the longitudinal axis of the pipe was varied for the cylindrical indenters. The longitudinal orientation was the primary focus of the study. The transverse orientation was used for 6 in. and 12 in. indenters. Longitudinal and transverse Type BH dents behaved similarly in the experimental program. Thus, short transverse dents were not modeled. Figure 4-2 provides an example of each indenter orientation using the Type A indenter.

Dent restraint was also modeled to represent a settlement induced or unyielding dent. The main variable of restraint is the flexibility of the indenter. Two simple methods of restraint were used. In the first case, the restraint remained rigid by forcing zero displacement of the restraint. In the other case, the restraining force remained constant throughout pressure cycling allowing rebound during cycling. The two cases represent upper and lower bounds of restraint flexibility. The first case represents a rigid restraint with no flexibility. All restrained or settlement induced dents have some degree of flexibility. The second case represents a very flexible restraint. It allows rebound without a change in restraint force. The restraining force of restrained dents increases with pressure with elastic behavior of restraint force and rebound. The behavior of actual restrained dents is bounded by these two cases.

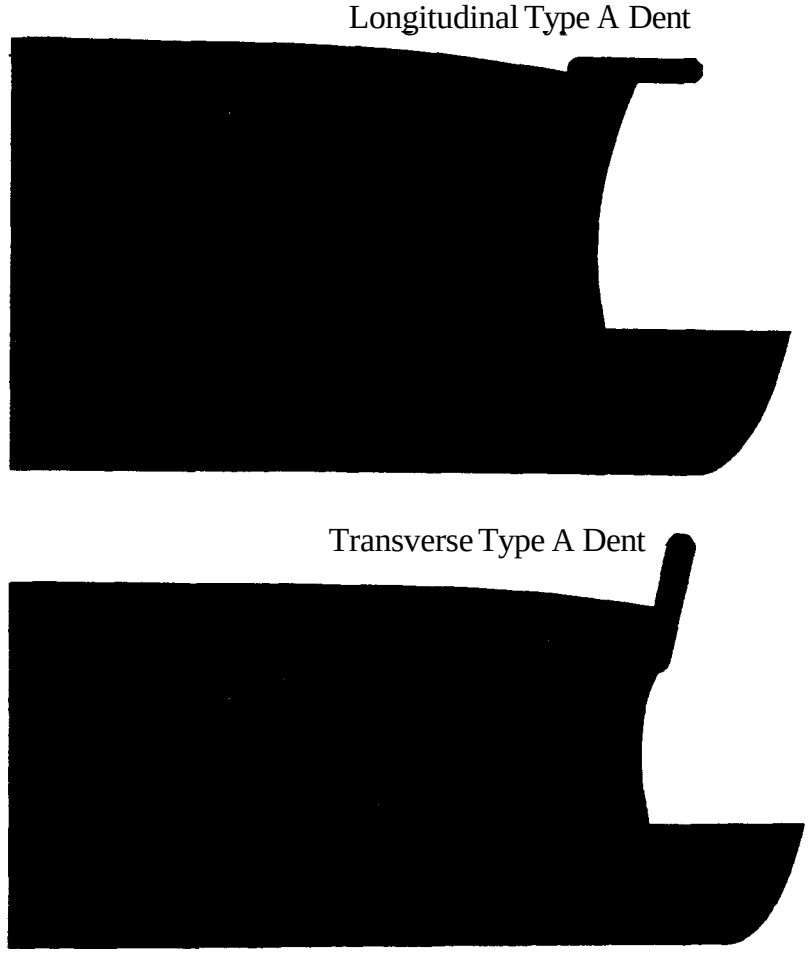

Figure 4-2: Indenter and dent orientation for finite element study.

4.2.2 Pipe Parameters

The pipe parameters modeled include diameter (D), thickness (t), pipe grade, longitudinal stress, pipe support, and pressure at indentation. The range of diameters modeled is fiom 12 in. to 48 in. For each diameter, several values for thickness were modeled. The pipe models will be named based on the outside diameter in inches followed by the thickness given in eighths of an inch. For example, Pipe 18-3 represents an 18 in. outside diameter pipe with a thickness of 3/8 in. Different pipe grades were modeled. The grades are based on API Spec. 5L. The experimental program used pipe specimens with API grades of B, X42, and X60. Tension tests of pipe specimen coupons were performed to determine the yield stress for the different grades

(see Sec. 3.9.7). From this data, three different stress-strain curves were developed to model the three MI grades. The specification gives the required minimum yield strengths for line pipe. The tension tests all gave higher values. In order to better estimate the behavior of pipelines, the higher yield strengths were used in the models. The yield strengths of the different grades are given in Table **4-3.** The three stress-strain curves fiom the experimental program for the three grades modeled are given in Fig. **4-3**

Table 4-3: Yield strength modeled in the finite element analysis.

API Spec. Grade	Minimum Yield (ksi)	Actual Yield Strength (ksi)
B	35	**50**
X42	**42**	**50**
X60	**60**	**60**

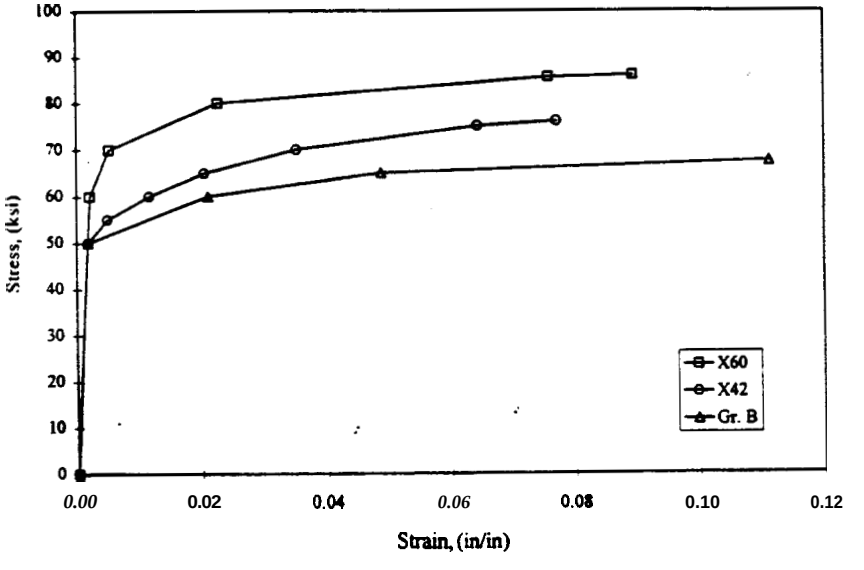

Figure 4-3: **Stress strain** curves modeled in the finite element analysis.

Two levels of longitudinal stress were investigated, fifty and thirty percent of the transverse or hoop stress. The fifty percent stress level is indicative of pipes or pressure vessels of finite length, with end caps. The longitudinal expansion of the pipe under pressure loading is unrestricted. This condition best models the pipe specimens used in the experimental program. For continuous pipelines, the longitudinal expansion or strain is reduced due to pipe skin friction of the soil, rigid thrust blocks, or supports. A design value of thirty percent of the transverse stress is typically used.

The longitudinal stress level is an influential parameter since it affects the stiffness of the pipe wall to denting. For a plate element, an increase in a tensile membrane stress increases its bending stiffness.

Different methods of support were modeled during the indentation process. The soil surrounding a buried pipe stiffens the pipe cross section during indentation. The soil limits the cross section from deforming to an elliptical shape and is a function of soil stiffness. A pipe dented above ground without the support of soil will be more flexible. The methods of support modeled during indentation are given in Fig. 4-4. Support Type A is the primary support method used to model the dent and pipe parameters. Support Type B was modeled to see how support conditions can change the behavior of dents. The stiffness provided by pipe support is bounded by the two support types modeled. The force required to achieve the same dent depth will increase when support conditions change from Type A to Type B. The support mechanism for the experimental test program involved a wooden saddle. It was used to prevent plastic deformation of the supporting area of the pipe during indentation. The indenter forces recorded for the test specimens should be bounded by the values for the two support types modeled.

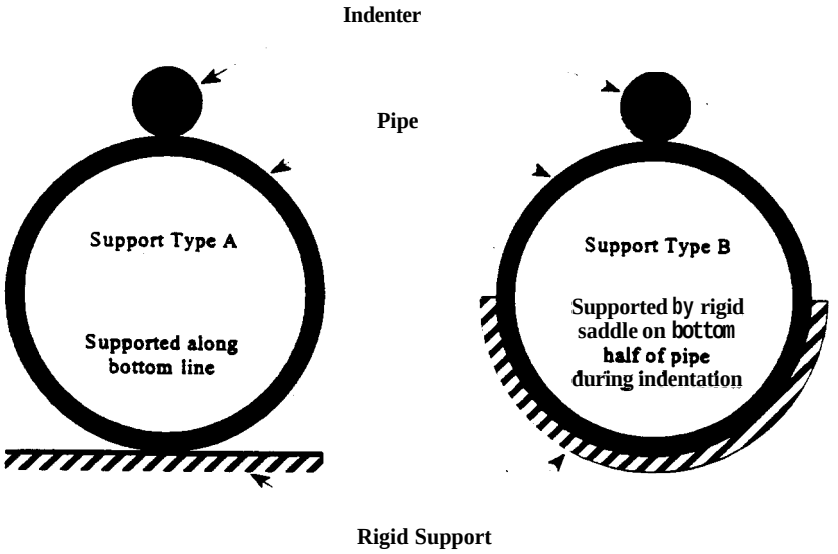

Figure 4-4: Support conditions modeled.

The internal pressure of a pipe affects indentation. The specimens for the experimental program were dented with zero internal pressure for safety reasons. A majority of the models were dented with zero pressure. A few models were dented at different pressures to see how the pressure at indentation influences the behavior of dents. The magnitude of the indenter force will increase with increasing pressure, which will affect the rebound characteristics.

The wide range of parameters covers most cases of dents in pipelines. A majority of the modeling was done for longitudinal unrestrained dents. The different parameters modeled for unrestrained longitudinal dents is given in Table 4-4. This set of parameters mainly involves D, t, and indenter length L. The smaller diameter pipes were modeled using grade X60. The larger diameter pipes above 24 in. were modeled using grade B. The grades chosen were based on availability. Higher grades are easily available for diameters up to 24 in. Larger diameter pipes are usually of lower grades. Transverse and spherical dents were modeled on 18 in. and 48 in. diameter pipes.

Table 4.4: Unrestrained longitudinal dents modeled in the finite element analysis.

	D, (in.)					
t, (in.)	12	18	24	30	36	48
0.250	A, BH, G,	A, BH, G,	A, BH, G	A, BH, G	A, BH, G	
0.375	A, BH, G,	A, BH, G,	A, BH, G	A, BH, G	A, BH, G	A, BH, G,
0.500	A, BH, G,	A, BH, G,	A, BH, G	A, BH, G	A, BH, G	A, BH, G,
0.625			A, BH, G	A, BH, G	A, BH, G	A, BH, G,
0.750				A, BH, G	A, BH, G	A, BH, G,

A slenderness ratio is used to identify the slenderness of a specific pipe. The ratio is equal to the diameter divided by the thickness. The range of slenderness (D/t) ratios modeled is from 24 to 144 for the unrestrained longitudinal dents. The slenderness ratio is considered as a parameter to see if it has any correlations with any of the other parameters. The values of D/t modeled for the different pipe sizes is given in Table 4-5.

Table 4.5: D/t slenderness ratios modeled in the finite element analysis.

Diameter, D (in.)	Thickness, t (in.)				
	0.250	0.375	0.500	0.625	0.750
12	48	32	24	19	16
18	72	48	36	29	24
24	96	64	48	38	32
30	120	80	60	48	40
36	144	96	72	58	48
48	192	128	96	77	64

4.3 FINITE ELEMENT MODEL

4.3.1 Mesh Design and Behavior

A three-dimensional finite element mesh was used to model the denting of pipelines with ABAQUS v5.5. This included the initial denting to a predetermined depth, removal of the denting force, and cyclic pressure loading resulting in the elastic and plastic rebound of the dents. Text input files were created using a spreadsheet format, thus allowing a simple way to vary the parameters for the large number of models analyzed. Computation was performed on either of the two supercomputers Terminator and Cyclops at Texas A&M University. Terminator is a 24 processor SGI Power Challenge. Cyclops is a 16 processor Cray J90 Y-MP compatible system. Parallel processing was used on both supercomputers. Output fiom the models include text data and contour plots. ABAQUS Post was used on the Terminator to generate all model and contour plots. Computation time for all models was over 10,000 cpu hours between the two machines.

Only shell elements were used to create the pipe mesh. Therefore, through thickness effects were not considered. Linear and quadratic quadrilateral elements were used. Quadratic elements were initially chosen assuming they would give better results. Comparisons between quadratic and linear elements give similar results, but the linear elements showed better model convergence. Thus, linear shell elements were used for most models.

Divergence resulted when ABAQUS was not able to arrive at a solution for the model equations. A nonlinear solver was used to arrive at the solution of the model equations. Several iterations were usually required to solve the equations for each *step* increment of the model. If the nonlinear solver was unable to solve the equations, the step increment was reduced. The minimum *step* increment was *set* to 1E-05. If the solver was unable to solve the equations at this step increment, program execution would be terminated due to model divergence. The rate of convergence is influenced by the amount of deformation. Deeper dents required more iterations to complete model steps, thus requiring more computation time than shallow dents.

Element s4r is a linear 4-node doubly curved thick or thin reduced integration shell. Element s8r is a quadratic 8-node doubly curved thick reduced integration shell. All models used the same mesh of nodes. The linear meshes had four times the number of elements as the quadratic meshes, but both cases had the same number of integration points. Therefore, both element types should give similar solutions. Element s4r has one integration point. Linear quadrilateral and triangular rigid elements were used to generate the indenters.

All indenters modeled were symmetric in shape and orientation with respect to the principal axes of the pipe. Two planes of symmetry were used such that only one-fourth of a pipe is modeled. Only transverse and longitudinal oriented dents were used. The wire mesh in Fig. 4-5 is an example of a 24 in. diameter pipe with a Type A indenter prior to indentation. The entire model is shown. The length of the model is equal to three pipe diameters of the largest diameter modeled (48 in.). The length of the model ensures that end effects will not influence the behavior of the dented region. A shorter model length was initially chosen, but, the indentation process caused the entire short model to deform without localized deformation surrounding the indenter. Constraining equations were placed on the end of the short model to constrain the displacement to that of elastic expansion from pressurization. The end constraints artificially increased the stiffness of the pipe and caused convergence problems. Thus, the longer longitudinal pipe length was used.

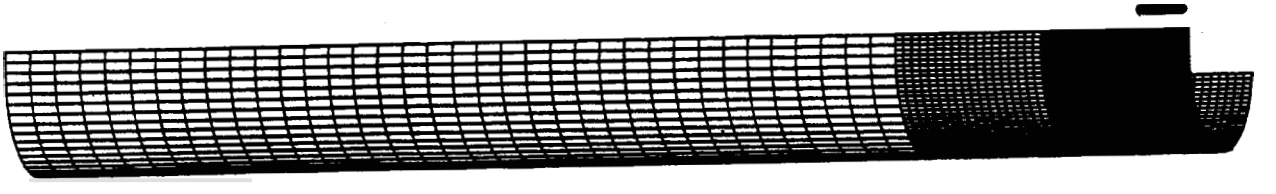

Figure 4-5: Undeformed 24 in. wire mesh with a Type A indenter.

A general mesh was developed to model the range of pipe and dent parameters. This allowed for the automation of developing input files and standardization of the output data for the various parameters. The length of the model remained constant at 144 in. for all models. Mesh refinement was used to increase the mesh density in the vicinity of the dent. Multi-point constraints were used to provide the transition between mesh densities. This is the standard method in ABAQUS for mesh refinement of first-order and second-order elements. An example of a multi-point constraint is given in Fig. 4-6 for mesh refinement of linear s4r elements. Each degree of freedom at node K is interpolated linearly from the corresponding degrees of freedom at nodes J and L. In this way, the displacement of node K is consistent with the displacement of the large element at mid-height. Linear and quadratic constraint equations were used on the meshes of elements s4r (linear 4-noded) and s8r (quadratic 8-noded), respectively. Refinement of the mesh was performed in both longitudinal and radial directions toward the dent contact region.

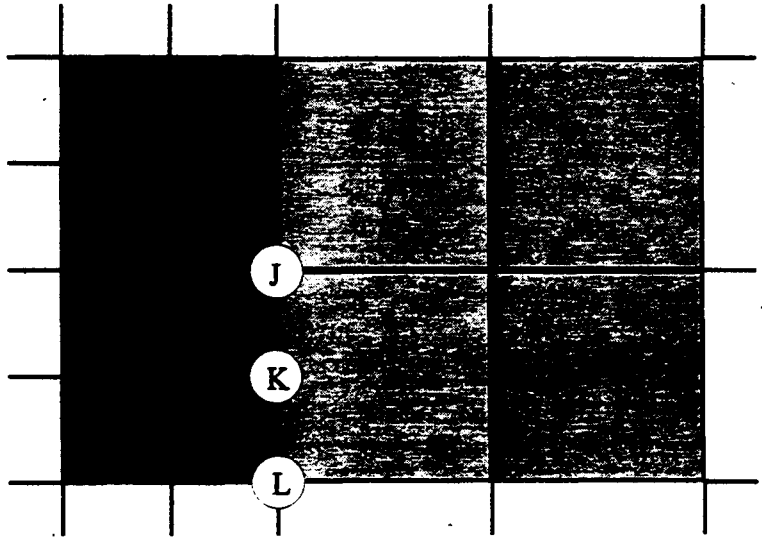

Figure *4-6:* Example of linear multi-point constraint.

The general layout of the mesh is given in Fig. 4-7. Four element sets were defined for mesh refinement. The nodal spacing in the longitudinal direction varies from 0.5 in. for element set S1 (dent vicinity) to 3 in. for element set S4 (end of model opposite the dent). The nodal spacing in the other direction was based on degrees of rotation from 0° to 180°. The range of

degrees per node is fiom 1.5° for element set S1 to 6" for element set S4. The dimensions and number of elements for each of the element sets is given in Table 4-6. The pipe mesh consists of a total of 4,860 linear shell elements with 30,246 degrees of freedom. The total degrees of freedom for the model with an indenter and contact interaction is 37,719. The largest ratio of element dimensions for all diameters of pipe modeled for element sets S1, S2, and S3 is 3.18. The maximum ratio is 4.78 for the element set S4, the region furthest away fiom the dent. The magnitudes of the ratios of element dimensions are not high enough to affect the behavior. Boundary conditions were applied to the four node sets TOP, BOT, RING1, and RING2. Node set TOP goes from node A to node F. Node set BOT goes from node C to node G. Node set RING1 goes radially from node A to node C. Node set RING2 goes radially from node F to node G. The location of nodes and element sets is also shown in a model plot of Pipe 18-3 with a Type A indenter in Fig. 4-8.

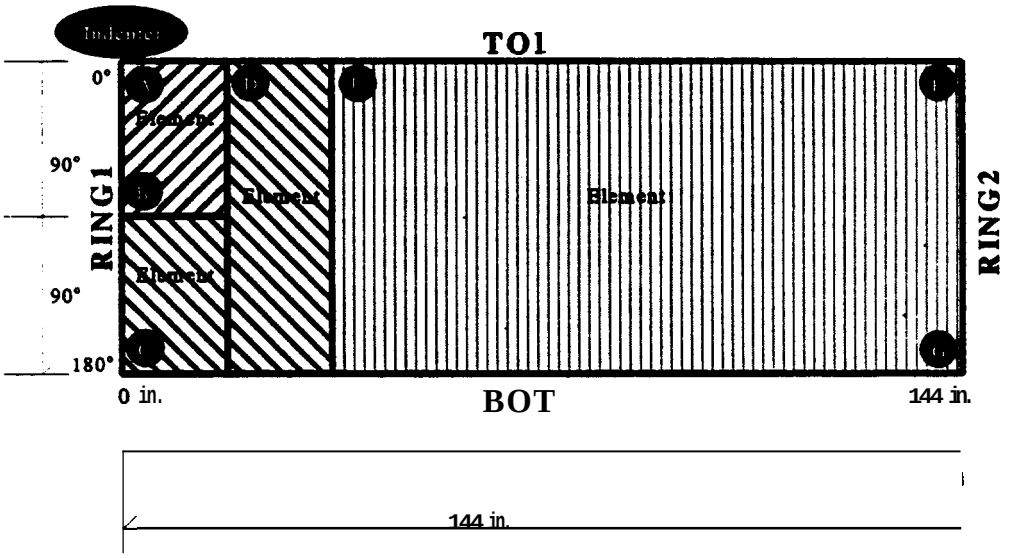

Table 4-6: Element set dimensions for linear S4R mesh.

Element Set	Dimensions		Number of Elements		
	Element	Element Set	Long.	Radially	Total
S1	0.5 in. by 1.5°	18.0 in. by 90.0"	36.0	60.0	2160
s2	1.0 in. by 3.0"	18.0 in. by 90.0"	18.0	30.0	540
s3	1.0 in. by 3.0"	18.0 in. by 180°	18.0	60.0	1080
s4	3.0 in. by 6.0"	104 in. by 180°	36.0	30.0	1080

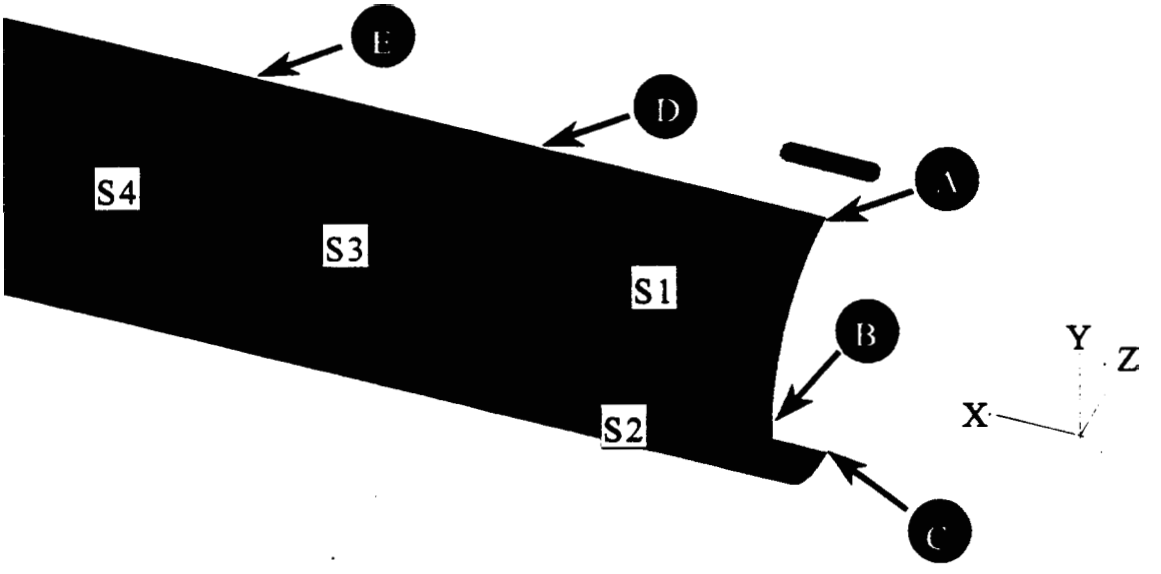

Figure 4-8: Model plot showing nodes and element sets.

Boundary conditions were prescribed to prevent rigid body motion of the model when subject to the indenter force and to account for the planes of symmetry. Reaction boundary conditions were given to node sets BOT and RING1. Node set BOT gives support in the Y direction. This was used as the reaction of the pipe for the indenting force. Node set RING1 gives support in the X direction. Node sets TOP and BOT have fixed boundary conditions of displacement in the Z direction and rotation about the X axis to account for symmetry.

Additional rotational boundary conditions were applied to RING1 and RING2 about the Y and Z axes.

The contact modeling of the rigid indenter and deformable pipe mesh was performed using a contact pair approach in ABAQUS. This method uses contact of surfaces to force displacement compatibility between the surface of the indenter and the pipe wall. A rigid surface was defined using the rigid elements available for this approach. This surface comprised of linear rectangles and triangles is automatically smoothed in ABAQUS. A contact node set was defined to represent the deformable pipe mesh using the nodes from element set S1. The rigid surface contains a reference node which was given displacements to move the indenter into contact with the pipe. This provided a simple method to make dents of specific depths. As the indenter moves into the pipe wall, the number of nodes in contact increases as the pipe mesh deforms to the shape of the rigid indenter. Using contact surfaces based on node sets can cause slight overclosure between the surfaces. This overclosure is insignificant for the mesh of shell elements since local contact plasticity of the pipe wall is not considered.

While a saddle support was used during indentation for the experimental specimens, no saddle was modeled during the indentation process. A saddle will increase the stiffness of the pipe cross section, thus reducing the cross section deformation towards an elliptical shape. For a given dent depth, this will increase the indenter load and local dent curvature. The models should have lower indenter forces as compared to the test specimens. Higher amounts of initial dent rebound are also expected from the global rebound of the elliptical shape.

Elasto-plastic behavior was given to the shell elements. Stress and strain values were used as input to define the elastic yield point and plastic behavior. Since large values of strain occur during indentation, the nonlinear step option was used in ABAQUS to model the pipe using large displacement theory. This option includes the effect of large displacement. The s4r shell element uses a fully nonlinear formulation.

The internal pressure was applied to the pipe model using a combination of pressure and concentrated loads. Membrane hoop stress was developed in the mddels by using a pressure load acting on the surface of the shell elements. The value of the pressure load had to be modified to account for the wall thickness, since the nodes of the models were based on the pipe outside diameter. While pressure loading acts normal to the inside surface of pipes, it can only be applied at node locations of shell elements. The input pressure for the model was adjusted by the ratio of inside to outside diameter to get the correct membrane (hoop) stress. The pressure load only applies to the hoop stress for the model. The longitudinal stress caused by pressurization was applied to the model using cbncentrated nodal loads in the X direction for node set RING2 (end of the model opposite to the dent).

4.3.2 Model History and Output

The models were analyzed in a similar fashion as the specimens were tested in the experimental program. That is, the pipe model is initially dented to a specific depth with zero internal pressure. If modeling an unrestrained dent, the indenter would next be removed, and the model would undergo elastic rebound. If modeling restrained dents, restraint flexibility would be defined at this point. Next, 'the model would undergo incremental static pressurization' to the design pressure. Then, the model simulates three pressure cycles such that equilibrium of the final dent depth is achieved. Incremental static pressurization was again performed to get stress, strain, and displacement output at various pressures. The pressure history used for input is based on percent of the pressure to cause the pipe to reach the specified minimum yield stress of the pipe grade, where the design pressure is 70 percent of the pressure to cause the membrane hoop stress to reach yield. The pressure was statically increased to 110 percent of the design pressure (77 percent yield pressure) as in the experimental test specimens.

Output fiom the models includes stress, strain, displacement, and indenter force. Stress, strain, and displacement data was recorded for the elements bordering node set TOP along the full length of the model. Stress and strain data was recorded in the transverse and longitudinal directions of the pipe at the outside and inside surfaces. Displacement data was also recorded for

node set **RING1** to show the change in shape of the cross section of the pipe at the center of the dent. The indenter force was recorded during indentation and cycling of restrained dents.

Each pipe model was dented to five predetermined depths fiom five to fifteen percent. **This** was accomplished in one model input file. A restart file was created in **ABAQUS** for the five model steps representing the five dent depths. Removal of the indenter and pressure cycling was performed in five additional files, one for each dent depth. Each of these files was given the model history fiom the appropriate step in the restart file to start rebound fiom the predetermined initial dent depths. **Thus, six** inputs files were used to model five different dent depths in each pipe for each dent **type.** A diagram showing the six model inputs files is given in Fig. 4-9.

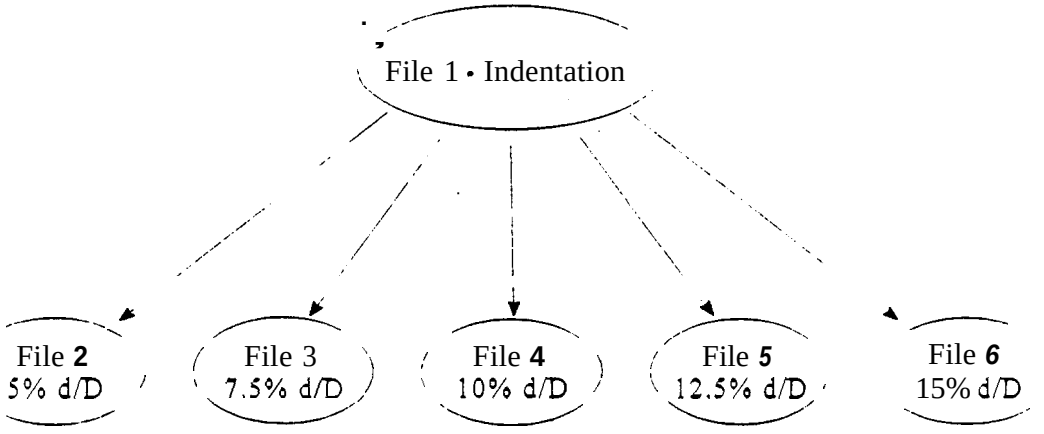

File 1: Incremental indentation to depths of **5,** 7.5, 10, 12.5, and 15% d/D
File 2: Indenter removal and pressurization **of 5%** d/D initial dent depth
File 3: Indenter removal and pressurization of **7.5%** d/D initial dent depth
File **4:** Indenter removal and pressurization of 10% d/D initial dent depth
File ***5:*** Indenter removal and pressurization of 12.5% d/D initial dent depth
File ***6:*** Indenter removal and pressurization of **15%** d/D initial dent depth

Figure 4-9: Schematic **diagram** of typical input files for finite element analysis.

4.3.3 Problems Encountered with Models

In addition to divergence of some models, other problems were encountered. Contact between the indenter and pipe mesh sometimes did not occur. The output stress data from all of the models gave values above the highest stress value given in the stress-strain input data. Output displacement data for some models is incorrect.

Difficulties arose in contact modeling for a few of the models. In the model, the indenter is initially not in contact with the pipe mesh. In the first step of the model, the indenter is given a displacement in the Y direction such that it has contact with the pipe mesh. For a few models, the indenter would move through the pipe mesh without any contact. To solve the problem, small displacements were applied to the indenter in the X and Z directions before displacement in the Y direction. This usually solved the problem.

The output stress data gave higher than expected values. The elastic-plastic stress-strain curves used are given in Fig. 4-3. For grade X60, the highest stress is 86 ksi at a strain of approximately 9 percent. With the elasto-plastic behavior in ABAQUS, *strain* hardening occurs according to the defined input stress-strain points. Once the strain reaches the last point defined, the behavior is purely plastic. Thus, for grade X60 models, stress values should be a maximum of 86 ksi. Output stress data for the models with grade X60 gave values near 100 ksi as shown in Fig.4-65. These values are considerably higher than the expected value of 86 ksi. The discrepancy of the stress data is likely caused by the formulation of the model mathematically.

Values of strain in the contact region exceed 20 percent for some models. The large strain values were initially assumed to cause the high stress values, but high stress values were found for models with maximum *strain* values of 3 percent. Thus, the amount of deformation is not causing the stress discrepancy.

The elastic-plastic stress-strain behavior was modified for one model to give elastic-purely plastic behavior without strain hardening to see the effect of the stress-strain behavior on

the stress data. For the elastic-purely plastic model, the maximum stress level is equal to the yield point which was defined to be 60 ksi. Stress data fiom the model gave values up to 69 ksi. Thus, the input stress-strain behavior does not change the stress discrepancy.

The stress data recorded is for the inside and outside surfaces of the pipe wall. The shell elements used in the mesh were given three section points through the wall thickness. An increase in the number of section points should give more accurate results. The default number of section points for shell elements is five. One model was analyzed with eleven section points through the wall thickness. This model gave stress values near 100 ksi for grade X60, which is identical to the models with three section points.

The direct cause of the high stress values was not specifically determined but is probably related to the multi-dimensional state of stress and restraint. The specified yield values are the result of Uniaxial tension tests. Regardless, the performance of the models is considered acceptable. The stress data for the models above the yield stress is exaggerated. Thus, the stress ranges are larger than they should be.

Some models gave displacement results that are incorrect. This was noticed for displacement data along node set TOP. An example of the incorrect displacement is given in Fig. 4-10 for Pipe 30-2 with a 15 percent *d/D* Type A dent. The shape after final rebound has a displaced shape with a ripple or trough located about 10 in. away fiom the center of the dent. This incorrect displaced shape was noticed on a few models only at the deeper dent depths. The location of the trough is near the area of mesh refinement which is located 18 in. fiom the center of the dent. The mesh refinement is assumed to be the cause of the incorrect displaced shape. Boundary conditions and modeling with symmetry are not the *cause.*

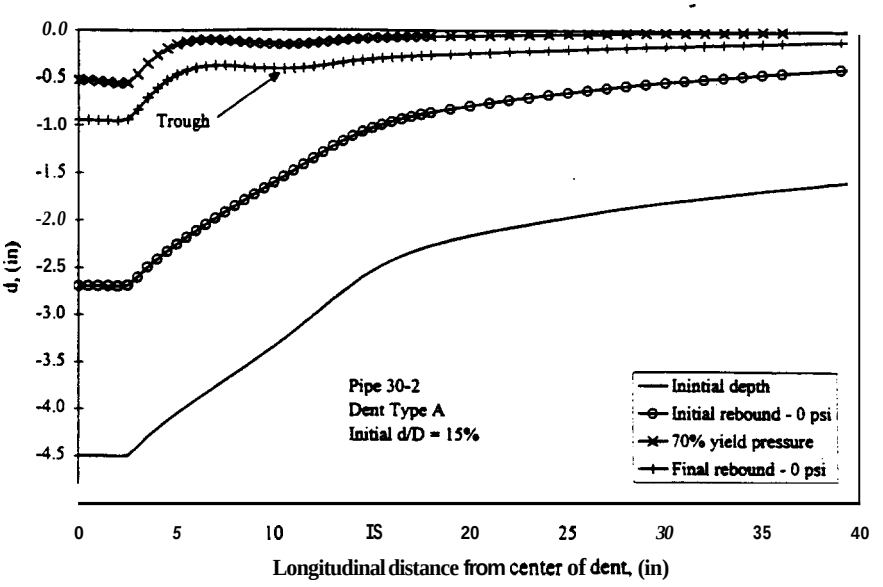

Figure 4-10: Longitudinal displaced shape of a 15 percent *d/D* Type A dent in Pipe 30-2 from indentation through final rebound.

4.4 REBOUND BEHAVIOR OF UNRESTRAINED LONGITUDINAL DENTS

4.4.1 Introduction

Two modes of fatigue failure can occur from unrestrained longitudinal dents in pipelines, corresponding to two different locations in or around the dent. The main parameters that affect the mode of failure include dent length, diameter, thickness, and dent depth. For the purpose of this investigation, the two modes of failure are designated as Mode 1 and Mode 2. Mode 1 dents develop fatigue cracks in the dent contact region, typically in the middle portion of the dent. Mode 2 dents develop peripheral fatigue cracks outside of the dent contact region. Mode 1 dents will be classified as long dents. Mode 2 dents will be classified as short dents.

Looking at the denting process in stages, the stress behavior of the dented region changes due to elastic and plastic rebound fiom removal of the indenter force and pressurization. After dent formation, the outside surface of the dent contact region has compressive residual stress. High plastic flow and material damage occurs in the dent contact region from the contact forces that develop on the outer surface of the pipe. Pressurization causes dents to rebound, with the longer dents having more rebound than short dents. The local rebound behavior of the dent contact region influences the stress distribution of the dent.

Typical transverse stress distributions found in short and long dents are illustrated in Fig. 4-11. Idealized linear elastic stress distributions are given for both the dent contact region and the dent periphery. At the maximum dent depth, the outside transverse stress in the contact region is highly compressive while the periphery is tensile, but of a lower, absolute magnitude. With pressurization, the flexibility of long dents allows the contact region to go from what was originally a compressive state of stress to that of tension, thus becoming susceptible to fatigue damage. The peripheral region also experiences a stress increase, but this is primarily due to the increase in hoop stress fiom pressurization. If the dent is short, the dent maintains its shape due to the increase in the dent stiffness. The lack of rebound maintains the compressive state of stress at the contact region, thus increasing the fatigue life of the contact region. This then forces

the crack formation location to the periphery of dent. Peripheral cracks must develop in a region without the benefit of a significant flaw resulting from contact damage caused by the indenting process. This increases the fatigue life when compared to long dents with cracks developing in the damaged contact region.

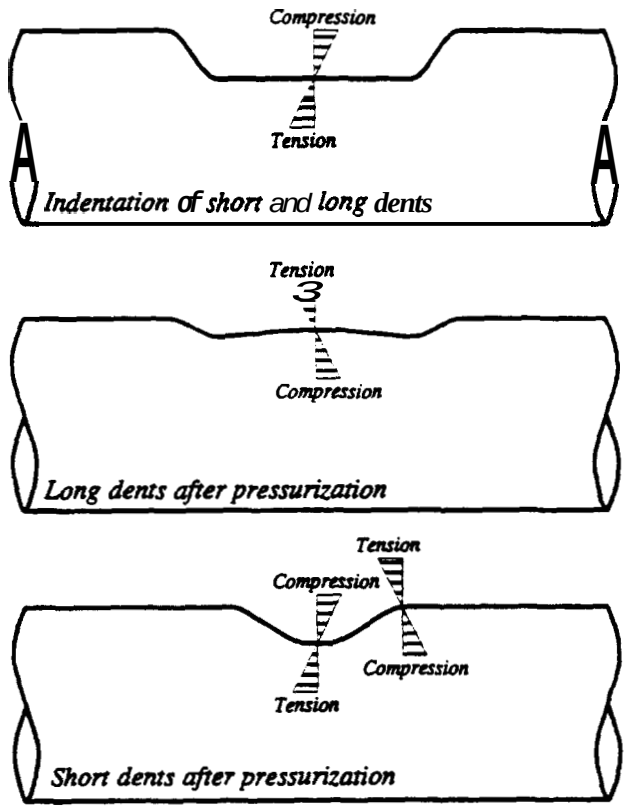

Figure 4-11: Typical transverse stress distributions of long and short dents.

It is a primary objective of this investigation to provide criteria for classification of dents with regard to fatigue strength. The behavior of longitudinal dents will be influenced by dent and pipe parameters, and include:

- Dent length
- Initial dent depth
- Final residual dent depth
- Pipe diameter
- Pipe thickness
- Pipe grade

Increasing dent length increases flexibility. Increasing dent depth increases dent stiffness due to the increased curvature of the contact region. Changes of the pipe parameters influence slenderness and pressure. The slenderness is related to the diameter and thickness. Increasing slenderness increases dent flexibility. The design pressure is influenced by diameter, thickness. and pipe grade. The magnitude of the design pressure for a pipe affects the local bending behavior of the dent contact region.

Dent length is the primary variable affecting the rebound behavior of dents. Dents with long lengths in general are susceptible to Mode 1 fatigue cracks in the dent contact region. Shorter dents are not susceptible to Mode 1 failures and develop Mode 2 peripheral fatigue cracks. The classification of a dent as short or long is mainly influenced by dent length. A Type BH dent with a length of 2 in. will most likely behave as a short dent. A Type G dent with a length of 12 in. will most likely behave as a long dent. The minimum dent length to cause long dent behavior is influenced by diameter, thickness, and the dent depth.

4.4.2 Dent Rebound Behavior

The rebound behavior of longitudinal dents is influenced by all 'dent and pipe parameters studied. Longer dents have more rebound than shorter dents. Slender pipes experience more rebound than thicker pipes. Dent depth also influences the rebound behavior. Rebound behavior can predict fatigue failure modes which can be verified by looking at stress distributions from the finite element modeling.

The formation of a longitudinal dent involves the entire indenter. The full length of the indenter has contact with the pipe regardless of dent length unlike a transverse indenter which can extend off of the pipe. The denting process causes the pipe to deform to the shape of the indenter in the dent contact region. Plastic deformation occurs along the entire area of indenter contact with the most damage at the edges of the indenter.

The deformed shape during indentation is given in Fig. **4-12** for Pipe **24-2** with a Type G dent. The figure shows the indenter and the elements along the top edge of the pipe mesh. The figure shows the general displaced shape with a zoomed-in view of the region of indenter contact. The contact region between the ends of the indenter is *smooth* and straight. **High** curvature is located at the end of the indenter where indenter contact ends. The entire contact region distributes the indenter force initially. The reaction forces between the pipe and indenter eventually concentrate at the ends **of** the indenter with increasing dent depth due to the deflected shape of the pipe. **Thus,** the highest contact damage is always **located** at the ends of the contact region. The plasticity from indentation will cause residual compressive stress to develop in the contact region. The deformed shape of the pipe at large dent depths may cause the center of the dent to loose contact with the indenter as shown in the enlarged portion **of** the figure. **This** contact behavior does not affect the fatigue behavior. It just shows **how** the ends of the contact region distribute **most** of the force which causes the highest plastic deformation at the ends.

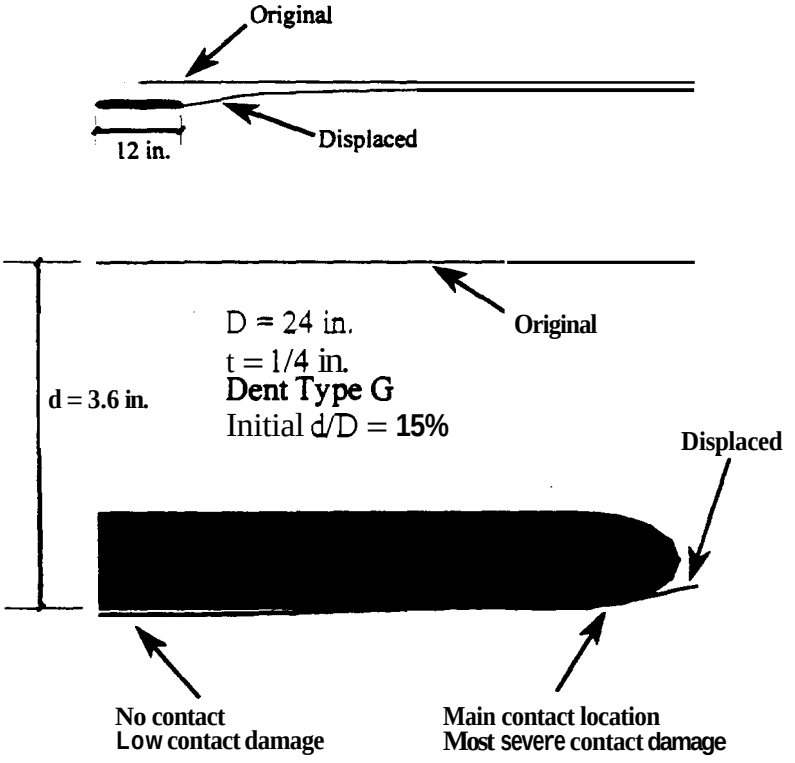

Figure 4-12: deformed dent shape at **indentation.**

Smaller dent types cause more plastic deformation than large dent types due to the reduction in contact area. This will cause smaller dent types to have higher compressive residual stress in the dent contact region. A decrease in indenter contact area makes smaller dents more susceptible to puncture through the pipe wall thickness.

The general rebound behavior of unrestrained longitudinal dents is largely influenced by the indenter length. The formation of a dent to its depth at the time of discovery or inspection occurs in three distinct stages:

- Initial formation to maximum dent depth
- Elastic rebound with indenter removal
- Plastic rebound under pressurization

The indenter initially creates a dent of a specific depth, identified as the initial dent depth at indentation. Removal of the indenter force causes a decrease in dent depth by elastic rebound of the dented area of the pipe. This stage is labeled as initial rebound. Internal pressurization then causes additional elastic and plastic rebound reducing the dent depth even more to the final dent depth. This is the permanent residual dent depth that will remain in the pipe. Model plots of the three stages of indentation, initial rebound, and final rebound show the rebound characteristics of dents.

Model plots for the three stages for indenter Types BH, A, and G on Pipe 18-3 are given in Figs. 4-13, 4-14, and 4-15, respectively. The viewpoint for the model plots is similar to the one in Fig. 3-11 of a test specimen from the experimental program where the longitudinal axis of the pipe is horizontal. Pipe 18-3 has a slenderness ratio of 48. The three model sets have an initial dent depth (d/D) of 10 percent. In Fig. 4-13, changes in dent depth from initial and final rebound are barely visible for the Type BH dent. The shape of the dented region remains the same throughout both stages of rebound. The rebound characteristics of the longer dent types are significantly different when compared to the Type BH dent. The influence of dent length on rebound behavior is apparent by comparing Fig. 4-13 and 4-14. The Type A dent undergoes more rebound than the Type BH dent, thus giving the Type A dent a lower final residual dent

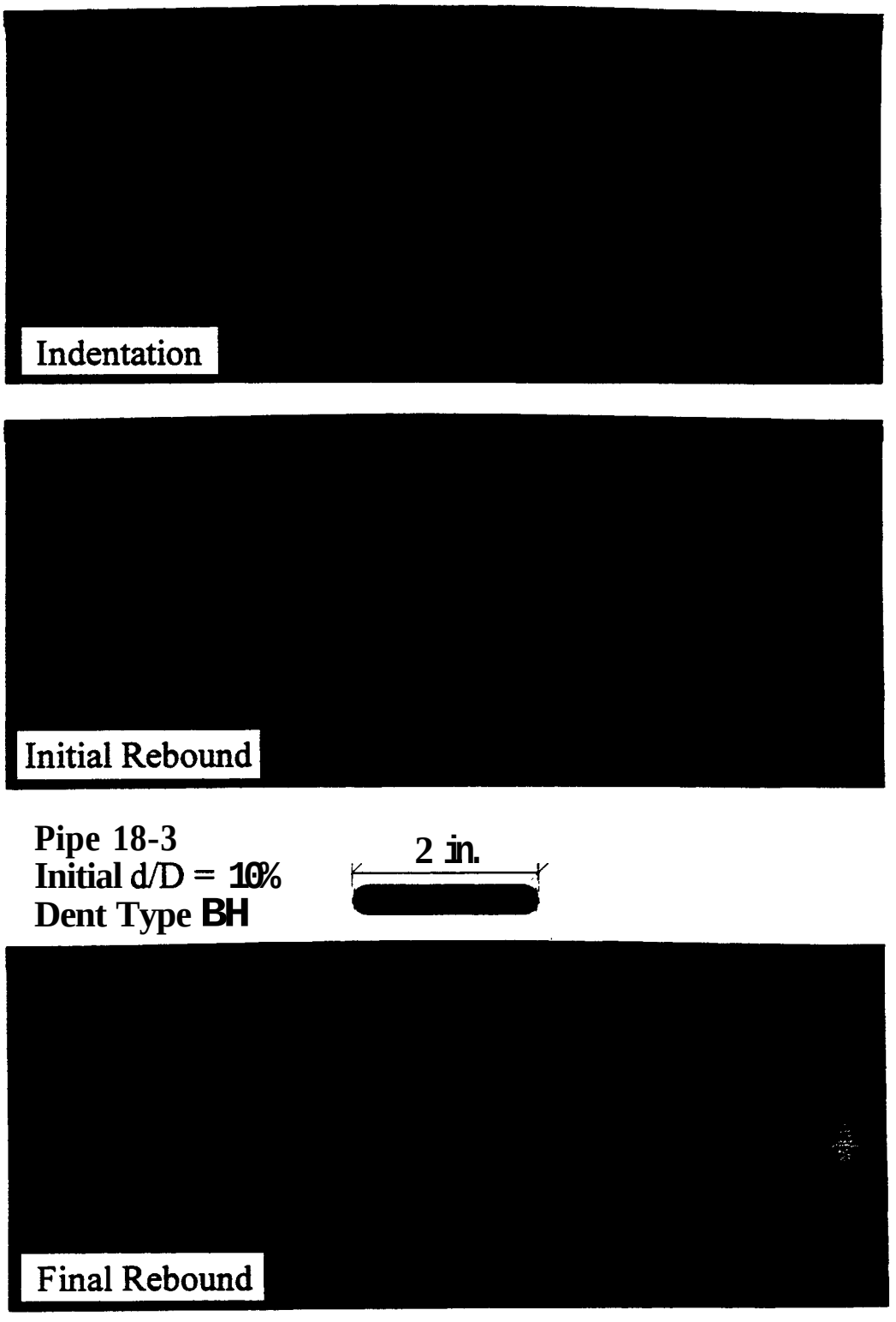

Figure 4-13: Dent Type BH **model plots of** indentation, initial rebound, and final rebound.

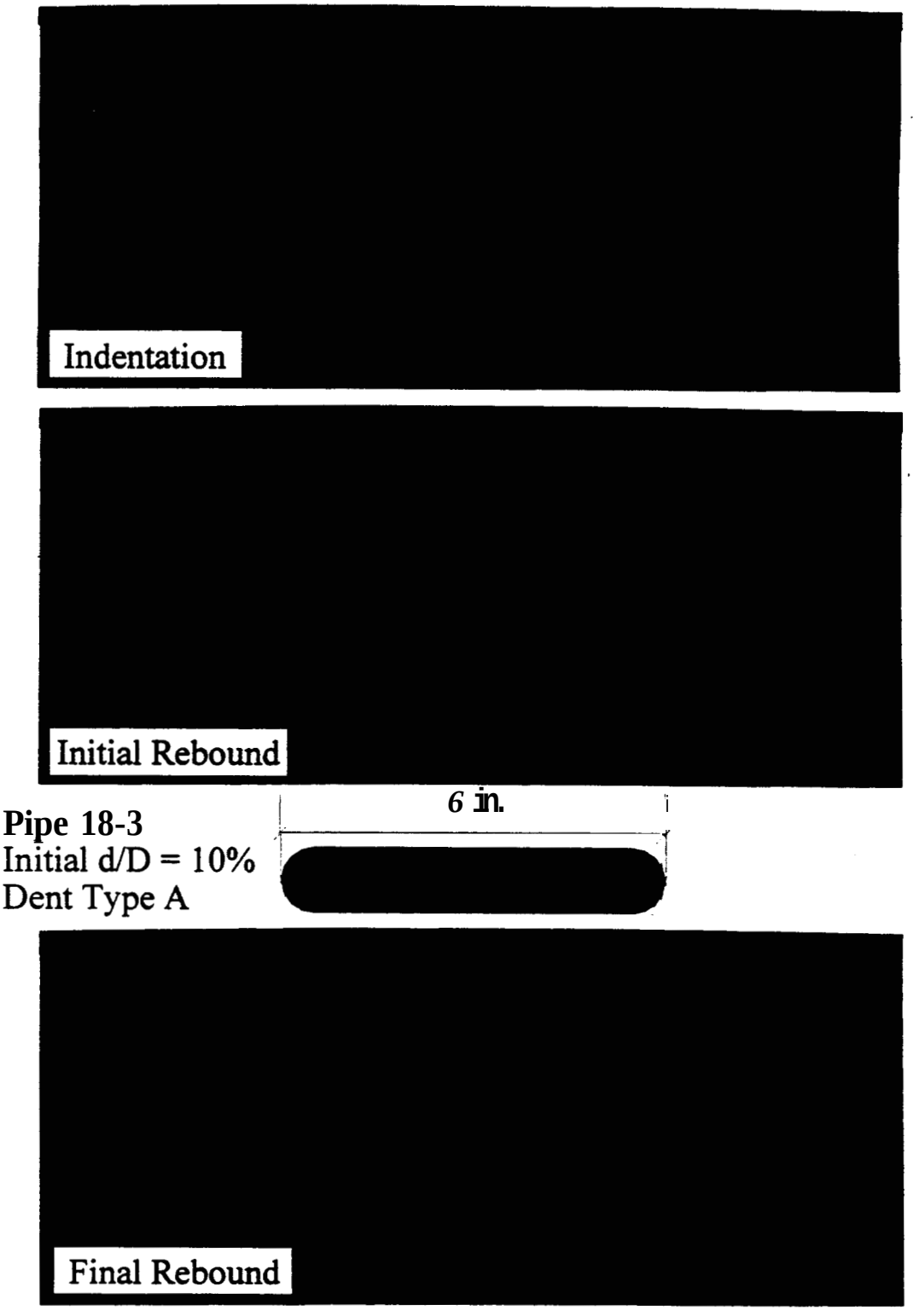

Figure 4-14: Dent Type A model plots of indentation, initial rebound, and final rebound.

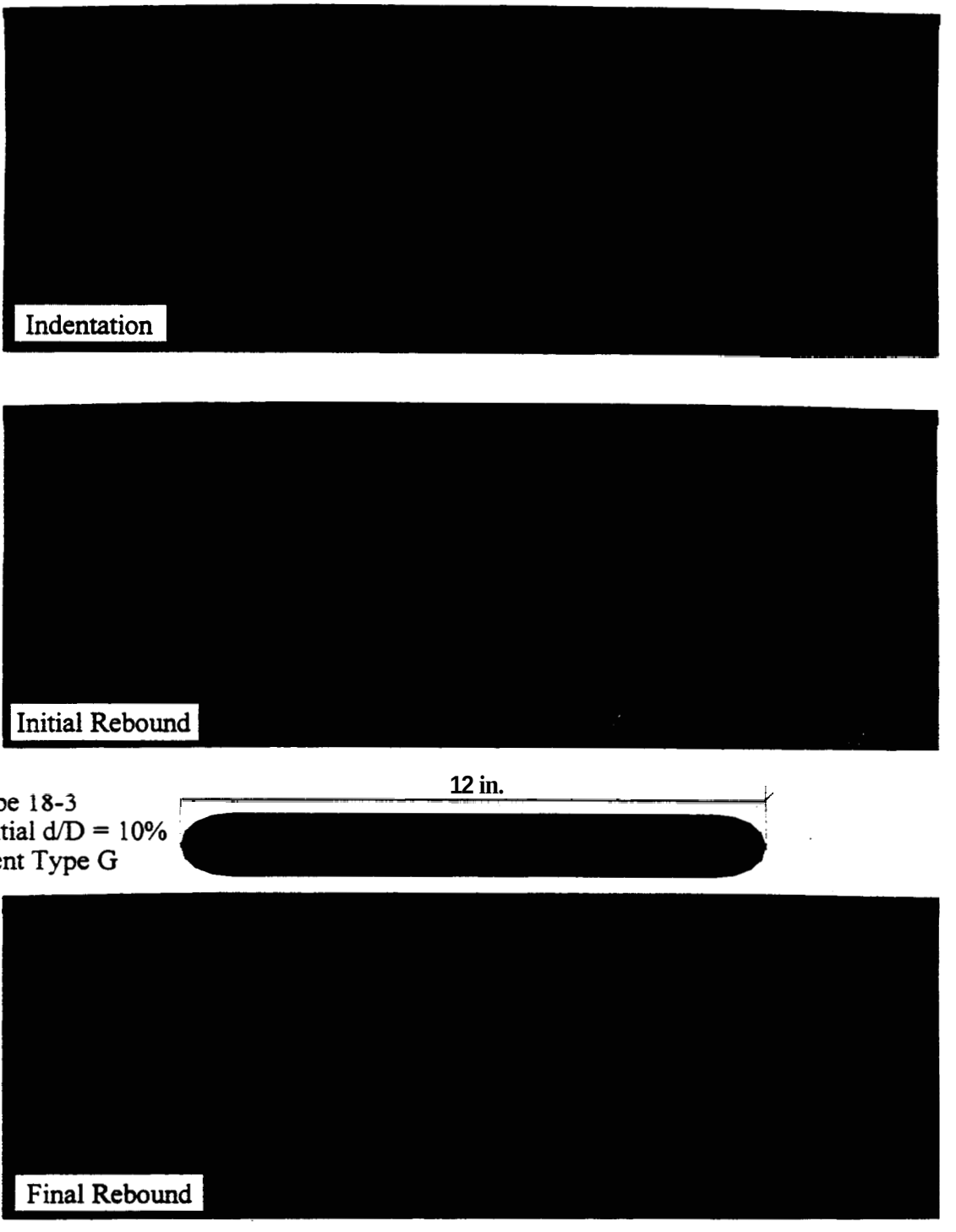

Figure 4-15: Dent Type *G* model plots of indentation, initial rebound, and final rebound.

depth. The Type G dent in Fig. 4–15, when compared to Fig. 4-14, shows how an increase of indenter length from the Type A dent leads to additional initial and final rebound. The change in dent length among the three dent types reveals that an increase in indenter length causes an increase in rebound, thus giving a decrease in final dent depth. Initial and final rebound is easily noticed visibly for the Types A and G dents unlike the Type BH dent.

The dent shape of both the Type A and G dents after final rebound is different from the dent shapes during indentation and initial rebound. The deformation of the dented region from contact by the cylindrical rigid indenter causes the contact region between the ends of the indenters to have a constant dent depth. The constant dent depth of the entire contact region remains during initial rebound as the indenter force is removed. The curvature of the dented regions is highest surrounding the edges of the indenter as was shown in Fig. 4-12 since the ends of the indenter distribute most of the denting force. Thus, the ends of the contact area have the highest stiffness due to the surrounding curvature of the dent shape. Curvature develops in the transverse and longitudinal directions surrounding the end of the indenter, whereas curvature at the center of the contact region is only in the transverse direction due to the constant dent depth between indenter edges.

Curvature surrounding the Type A dent of Fig. 4-14 is shown with a contour plot of the displaced shape after initial rebound in Fig. 4-16. The arrows represent directions of slope of the dented region. Since the contact region has a constant dent depth in the longitudinal direction, there is no curvature in the longitudinal direction between the ends of the indenter. Thus, the longitudinal direction of the contact region does not have any stiffness provided from the shape of the dent. The center of the dent will bulge with pressurization due to low longitudinal stiffness of the contact region. The tendency of a longitudinal dent to rebound with a bulge at the center of the dent is primarily influenced by the length of the indenter. Long dents are susceptible to this rebound behavior. Short longitudinal dents such as Type BH dents do not develop the longitudinal bulge due to the short dent length.

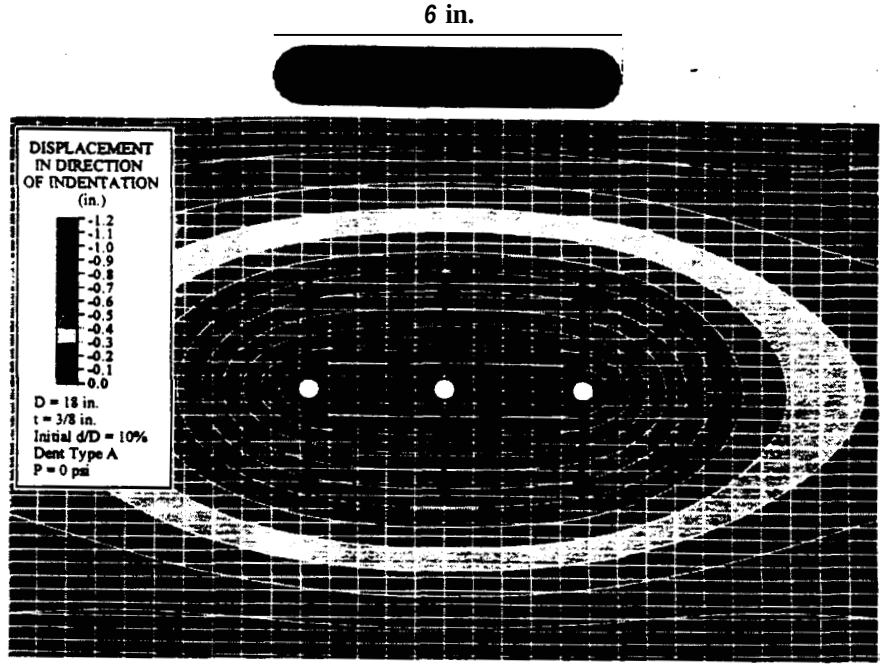

Figure 4-16: Contour plot of displacement in direction of indentation for pipe 18-3 after initial rebound for a Type A dent. Arrows represent directions of slope of the dent region.

The change in dent depth from indenter removal and pressurization is shown in Fig. 4-17 for Pipe 18-3 with Type BH dents. The initial dent depths rebound elastically from removal of the indenter force to the initial rebound depth. Pressurization to the design pressure causes elastic and plastic rebound. Removal of the internal pressure causes an increase in dent depth to the final residual dent depth due to elastic rebound. The difference in the final rebound depth and dent depth at the design pressure represents the fluctuation of dent depth during the service life of a pipe.

Rebound involves local and global elastic and plastic behavior. Local rebound occurs in the dented area of the pipe. Dented pipes become elliptical. Global rebound occurs when the elliptical shape is deformed back to the original circular cross section. Figures 4-18, 4-19, and 4-20 show the cross section displaced shape of the longitudinal center of the dent (node set RING1) for the stages of indentation, initial rebound, and final rebound. In Fig. 4-18, the increase in horizontal dimension from the original circular shape represents the global elliptical

displacement. Global elastic rebound with removal of the indenter force is shown by comparing the change in horizontal shape from the initial dent depth to the initial rebound dent depth in Figs. 4-18 and 4-19. Elastic and plastic global rebound occurs from pressurization. The horizontal displacement after final rebound is negligible.

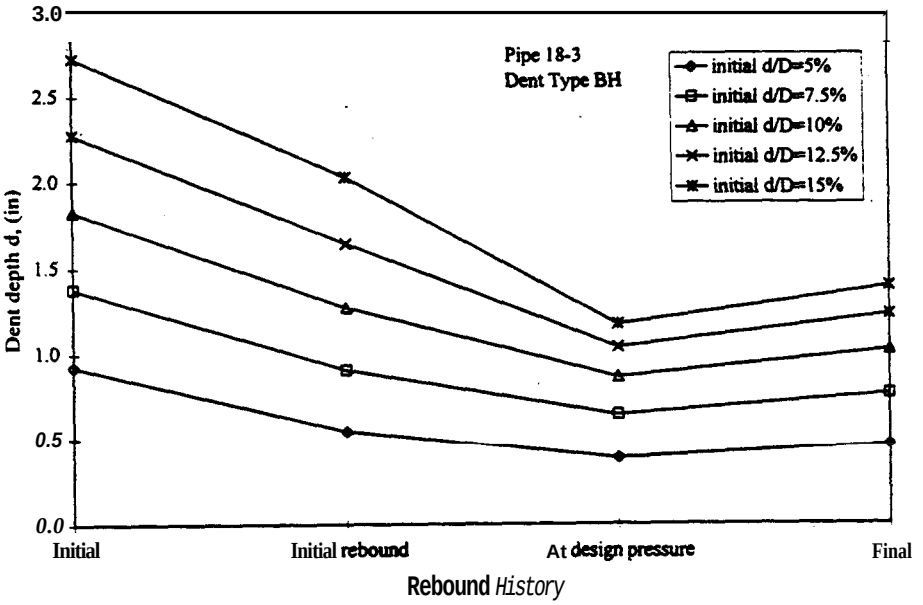

Figure 4-17: Rebound history of Type BH dent for Pipe 18-3.

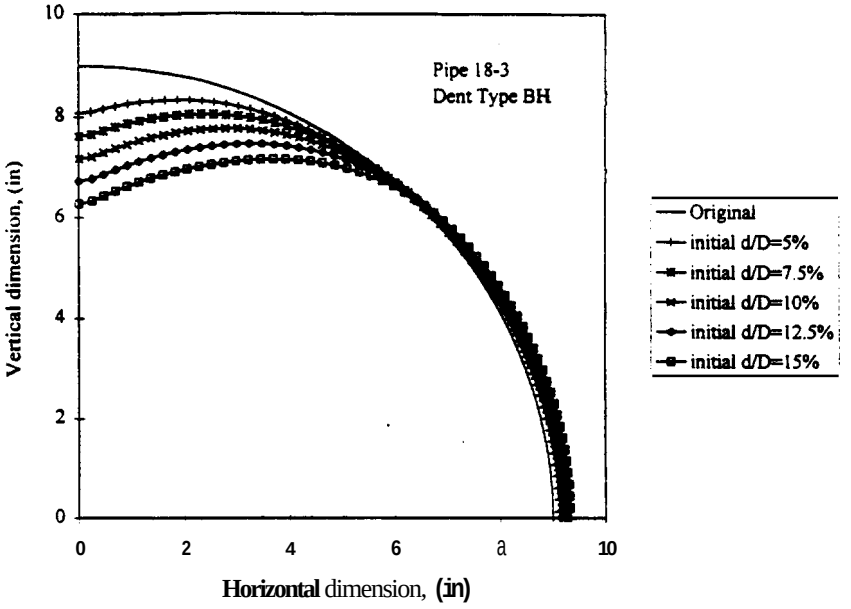

Figure 4-18: Type **BH dent displaced cross section at indentation for Pipe 18-3.**

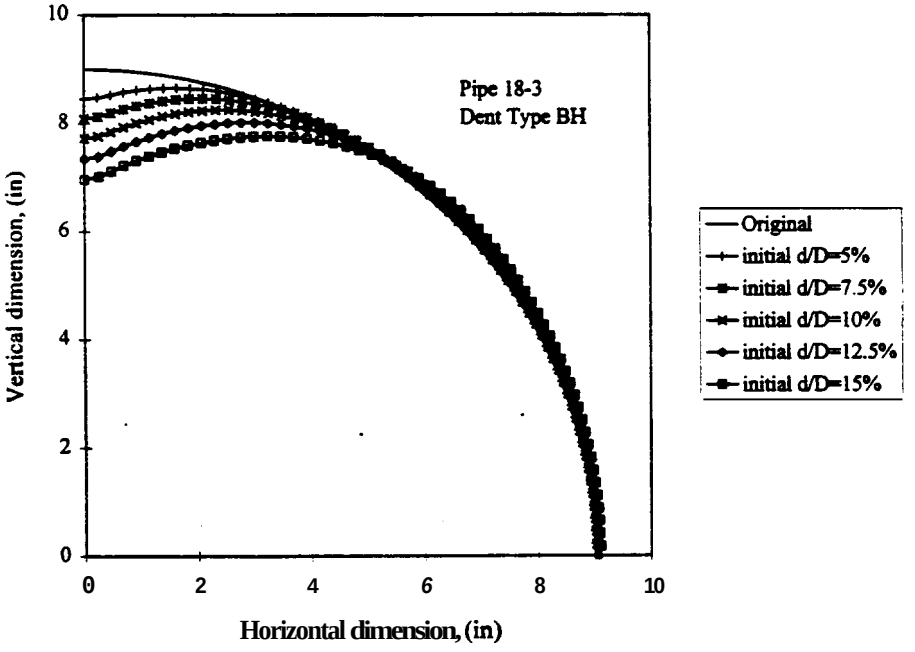

Figure 4-19: Type **BH dent displaced cross section *after* initial** rebound **for Pipe 18-3.**

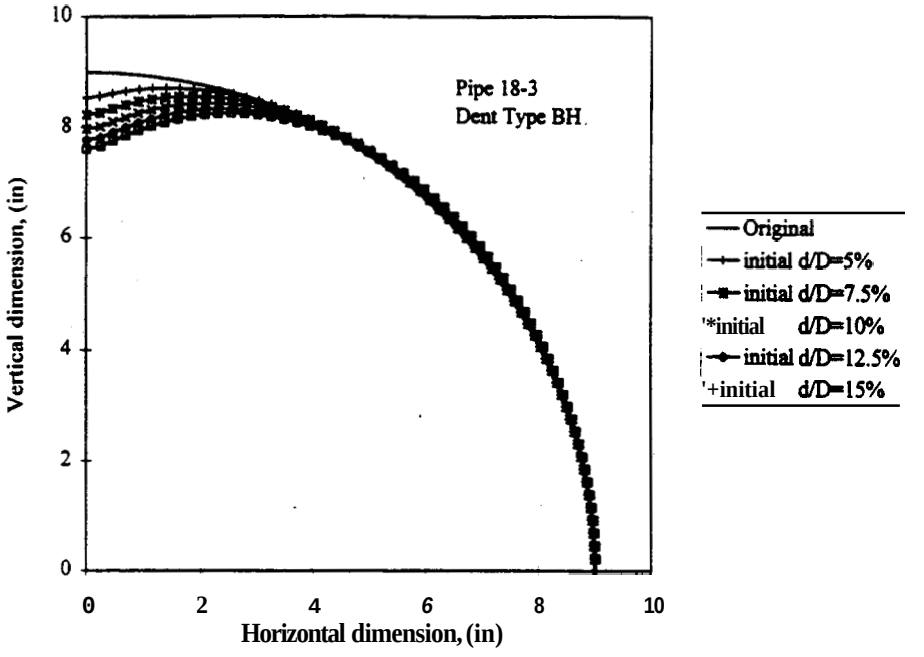

Figure 4-20: Type **BH** dent displaced cross section after final rebound for Pipe 18-3.

4.43 Dent Type A Rebound Behavior

Longitudinal unrestrained Type A dents have significant rebound. This was first noticed from specimens in the experimental program. Type A dents of different initial dent depths were found to have similar final dent depths after pressurization. This is due to the bulging rebound behavior of the longitudinal indenter contact region. Dent depth measurements were initially studied at the center of the dent, which has the smallest dent depth since it is the highest part of the bulge. These measurements were found to converge to a final rebound dent depth for significantly different initial dent depths. The largest values of dent depths for bulged dents are recorded at the ends of the indenter contact region which do not bulge. Depth measurements at these locations do not show the convergence of dent depth for different initial dent depths as compared to depth measurements at the center of the dent. For clarity, the different locations of dent depths recorded is given in Fig. 4-21. The figure represents a longitudinal section through the center of the dent.

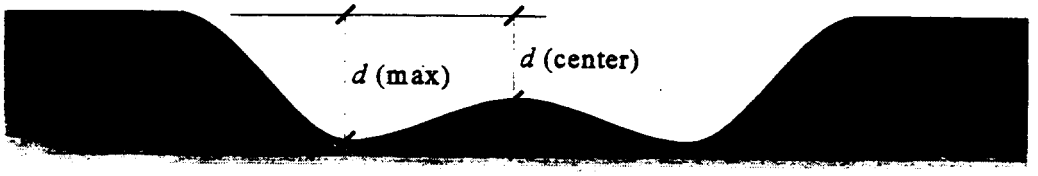

Figure 4-21: Locations of dent depth measurements for bulged longitudinal dents.

Displacement data was recorded along the longitudinal plane of symmetry for the models along node set TOP. The general rebound behavior of most pipe sizes with Type A dents is shown for Pipe 18-3. Figure 4-22 shows the shape of Type A dents at indentation prior to removal of the indenting force for Pipe 18-3. The five initial depths range from 5 to 15 percent d/D, in 2.5 percent increments. The initial rebound shape of the Type A dents is given in Fig. 4-23. The final rebound shape is given in Fig. 4-24. The entire contact region remains at an equal depth from indentation through initial rebound. Pressurization causes the bulge to develop. The dent depths at the center of the dent *after* final rebound are similar. Thus, depth data recorded at the center of the dent alone is not a useful measurement for predicting fatigue behavior strictly on dent depth. The dent depth measurements at the edge of the contact region increase with increasing initial dent depth as expected. These measurements can be applied to fatigue life prediction.

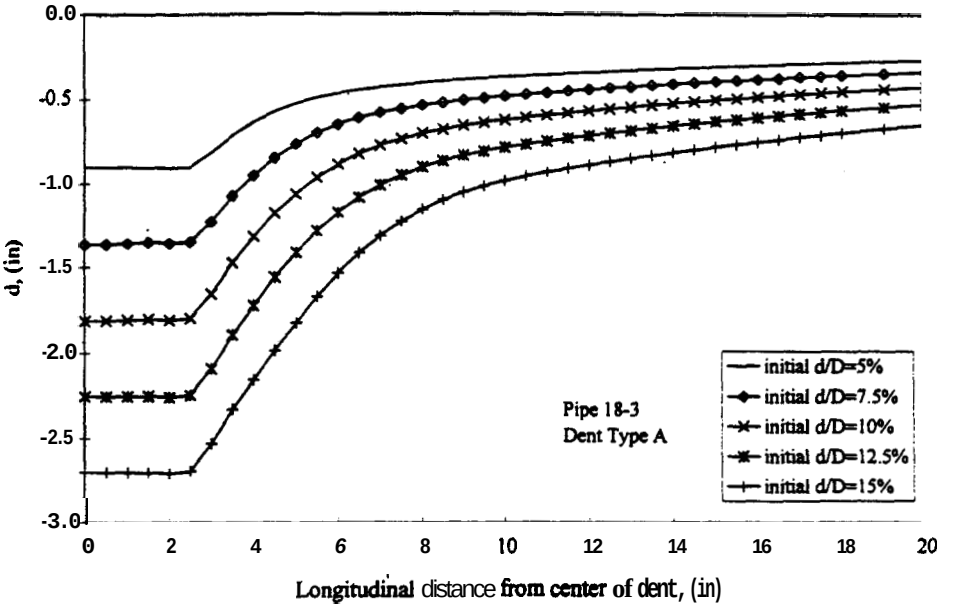

Figure 4-22: Type A dent depth at indentation for Pipe 18-3.

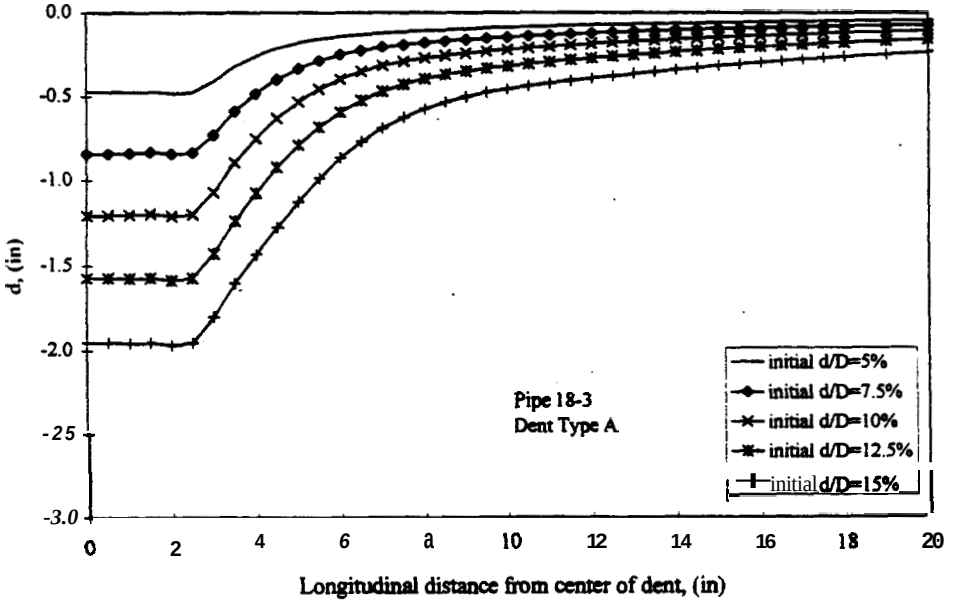

Figure 4-23: Type A dent depth after initial rebound for Pipe 18-3.

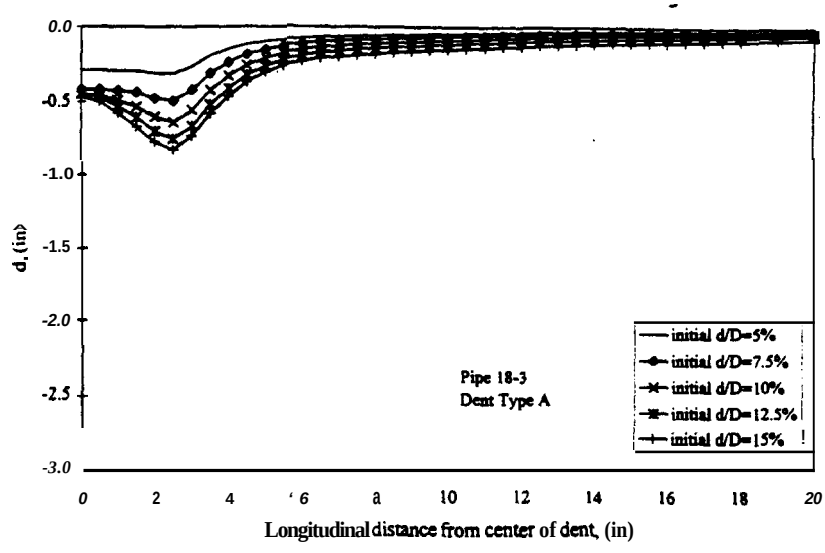

Figure 4-24: Type A dent after final rebound for Pipe 18-4.

Based on geometry of the final rebound shape of the Type A dents in Pipe 18-3, locations of fatigue crack development are easily predicted. The predicted failure location is at the center of the dent on the bulge. The rebound of the center of the dent suggests that compressive residual stress of the contact area is lost due to the bulging behavior as the bending stress on the outside surface reverses into tension. The curvature of the bulge is higher for the deeper dents. The amount of bulge curvature is related to the difference in dent depths between the largest depth at the contact edge and the depth at the center of the dent. The curvature of the bulge is related to plastic rebound. The deeper dents have more plastic rebound at the bulge which suggests a severe reduction of fatigue life based on increasing initial dent depth.

Formation of the bulge is influenced by initial dent depth, diameter, thickness, and pressure. The pressure can be directly related to diameter, thickness, and pipe grade. During initial pressurization of the first pressure cycle, it can be shown that dents with smaller initial depth bulge at lower pressures. For dents with deeper initial depths, the additional curvature

from increased indentation increases the stiffness of the dented region, thus requiring a higher pressure to develop a bulge. Therefore, an increase in initial dent depth prevents the formation of a bulge. In slender pipes, the reduced dent stiffness causes dents of all depths to form a bulge regardless of initial dent depth. In thick pipes, however, bulges may not develop in deeper dents due to the increase in dent stiffness of deeper dents.

Pipe diameter is the primary parameter affecting the bulge behavior of dents. Thickness and pipe grade have less influence. An increase in diameter lowers the design pressure of a pipeline. Bulging behavior is directly caused by pressure loading. A simple representation of the loading condition of pressure on a dent is given in Fig. 4-25. The springs simulate stiffness. The edges of the dent have more stiffness than between the edges due to dent geometry as discussed with Fig. 4-26. The area surrounding the dent region only has deflection from radial expansion with pressurization. The deflected shape caused by a bulge is similar to the deflected shape of a structural beam element subjected to a distributed load. For a distributed load, the bending stress of a simply supported beam is a function of the beam length squared. Thus, the bulging behavior of the dent contact region should be related to the dent length squared. An increase in thickness t increases the bending stiffness, but with an increase in pressure which in turn increases the bending stress of the contact region.

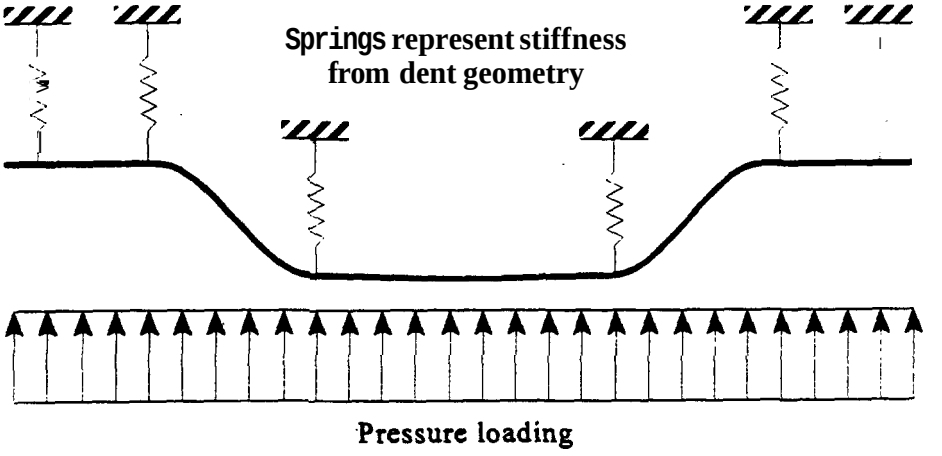

Figure 4-25 Representation of Pressure Loading on a Dent.

Larger diameter pipes with Type A dents are less likely to develop the bulging behavior. The final rebound shape of Pipe 30-4 with Type A dents is given in Fig. 4-26. Only the smallest initial dent depths of 5 percent and 7.5 percent d/D have a bulge in the center of the dent. The deeper dents do not bulge due to the increase in dent stiffness from the increase in dent depth. Comparing the rebound of Pipe 30-4 to Pipe 18-3 (Fig. 4-24) shows the influence of diameter on the susceptibility of Type A dents to the bulging rebound behavior. Pipe 30-4 has a slenderness ratio of 60 and Pipe 18-3 has a ratio of 48. Pipe 30-4 has a higher slenderness ratio, but does not have the bulging behavior of Pipe 18-3.

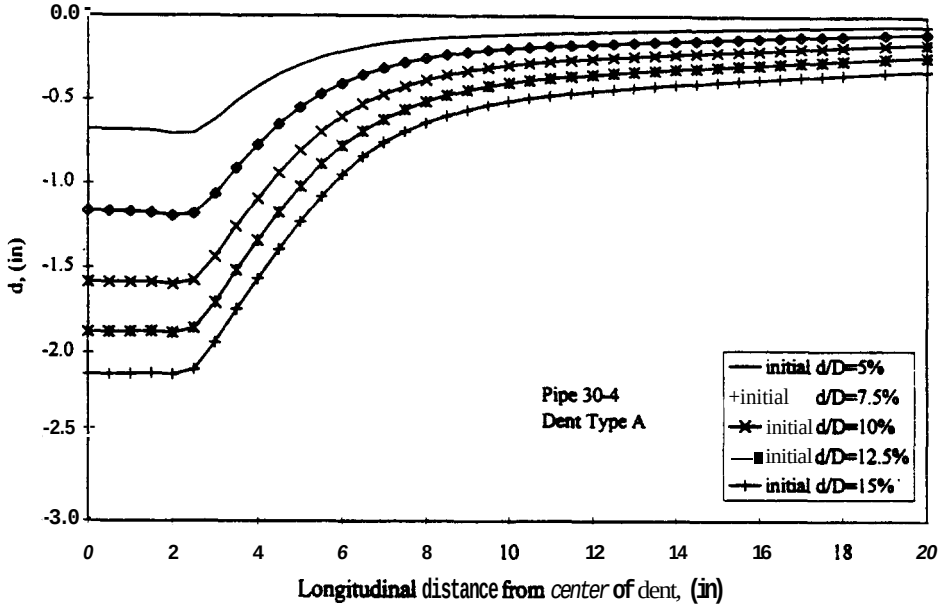

Figure 4-26: Type A dent after final rebound for Pipe 30-4.

The lack of dent bulging of Type A dents in large diameter pipelines suggests a transition in dent behavior from long dent behavior to short dent behavior as diameter increases. The long dent failure mode with crack initiation at the center of the dent may occur for large diameter pipelines, but the lack of center of dent bulging as compared to smaller diameter pipelines suggests that Type A dents in larger diameter pipelines have longer fatigue lives.

Diameter and thickness influence the amount of initial and final rebound that a dent will have. An increase in diameter causes an increase in rebound. An increase in thickness causes a decrease in rebound. These trends are verified with the dent depth data. The final rebound dent depths (percent d/D) of Pipes 12-2, 12-3, and 24-2 with initial dent depths of 10 percent d/D are 3.5, 4.5, and 2.0, respectively. The increase in thickness from 0.250 in. to 0.375 in. for the 12 in. diameter pipes results in an increase in final dent depth from 3.5 percent to 4.5 percent d/D. The increase in pipe diameter from Pipe 12-2 to that of Pipe 24-2 results in a decrease in final rebound dent depth from 3.5 percent to 2.0 percent d/D.

The change in dent depth from rebound was plotted in a variety of ways in an attempt to correlate rebound with the various pipe and dent parameters. Figure 4-27 is a graph of final dent depth (d/D) vs. initial dent depth (d/D) for all longitudinal unrestrained Type A dents for a pipe diameter of 12 in. Figures 4-28 and 4-29 give the same graphs for diameters of 30 in. and 48 in., respectively. Each figure shows that an increase in thickness increases the final dent depth. For each thickness, a linear relationship exists between the initial and final dent depth. This relationship was found for all diameters modeled which range from 12 in. to 48 in. All data series for all diameters have a linear trend with Y intercepts near the origin. Thus, a homogeneous relationship exists between initial and final dent depths for Type A dents on any initial dent depth for a specific pipe. The ratio of final to initial dent depth will be called the Rebound Ratio:

$$R_{rebound} = \frac{d_{final}}{d_{initial}} \qquad \text{Eq. (4-1)}$$

The homogeneous relationship requires the Rebound Ratio to remain constant for all dent depths for a specific pipe. Figures 4-30, 4-31, and 4-32 give graphs of Rebound Ratio vs. initial dent depth for 12 in., 30 in., and 48 in. diameter pipes, respectively. The graphs show that considering the Rebound Ratio as constant for different dent depths for a specific pipe is a reasonable approximation for all pipe sizes modeled.

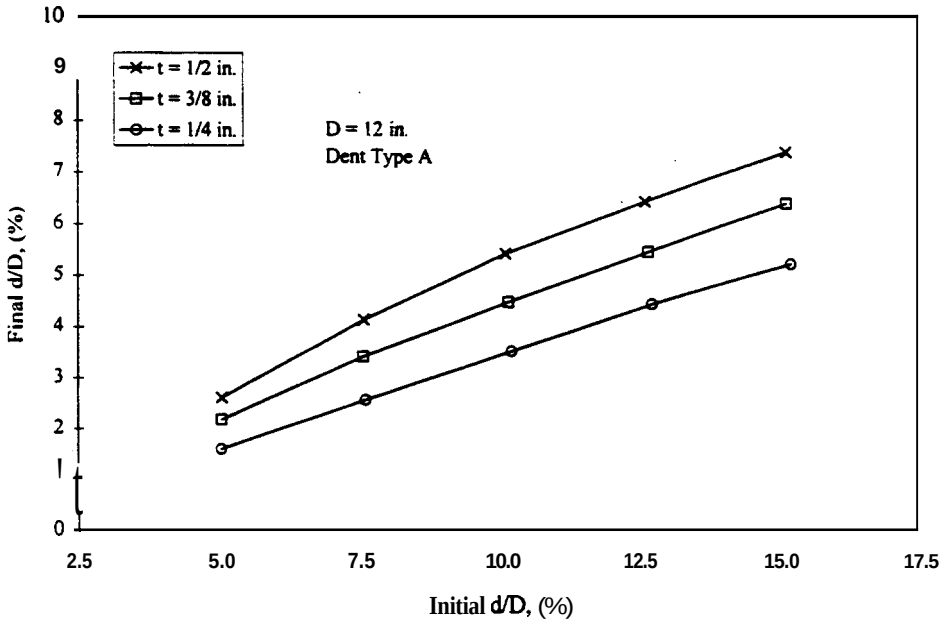

Figure 4-27: Final dent depth (*d/D*) vs. initial dent depth (*d/D*) for all Type A dents in 12 in. pipes.

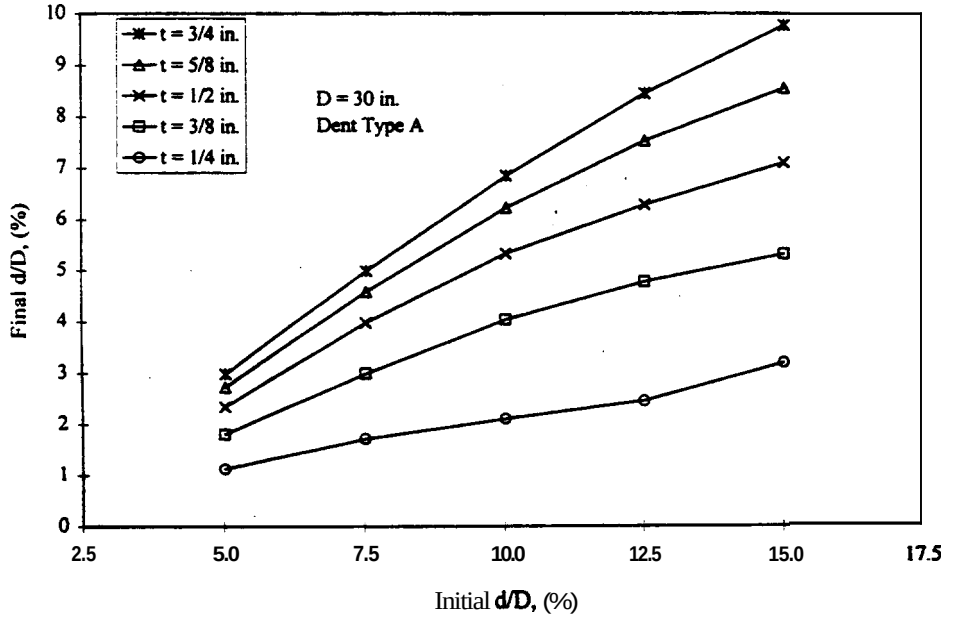

Figure 4-28: Final dent depth (*d/D*) vs. initial dent depth (*d/D*) for all Type A dents in 30 in. pipes.

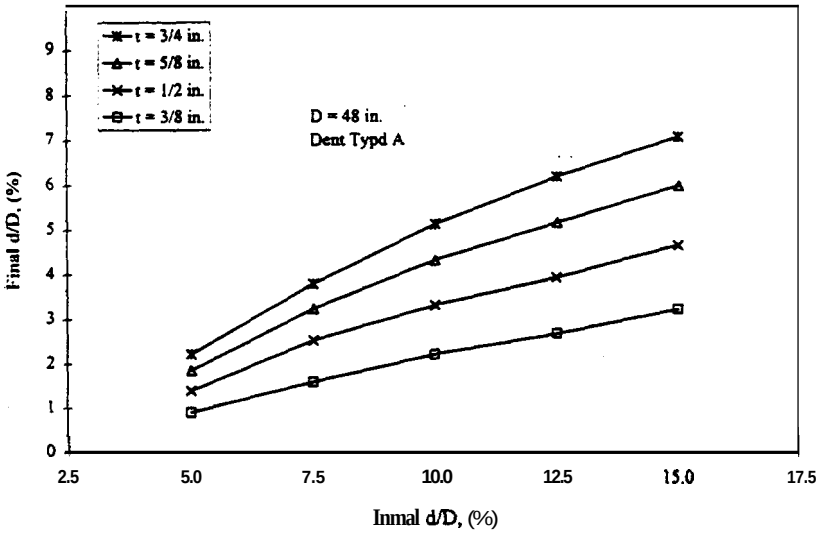

Figure 4-29: Final dent depth (*d/D*) vs. initial dent depth (*d/D*) for all Type A dents in 49 in. pipes.

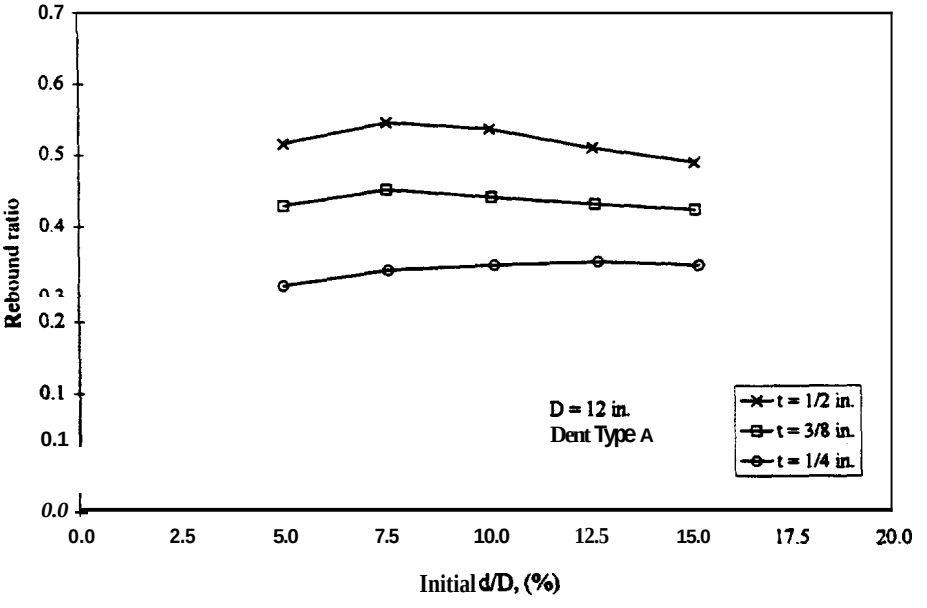

Figure 4-30: Rebound Ratio vs. initial dent depth (*d/D*) for all Type A dents in 12 in. pipes.

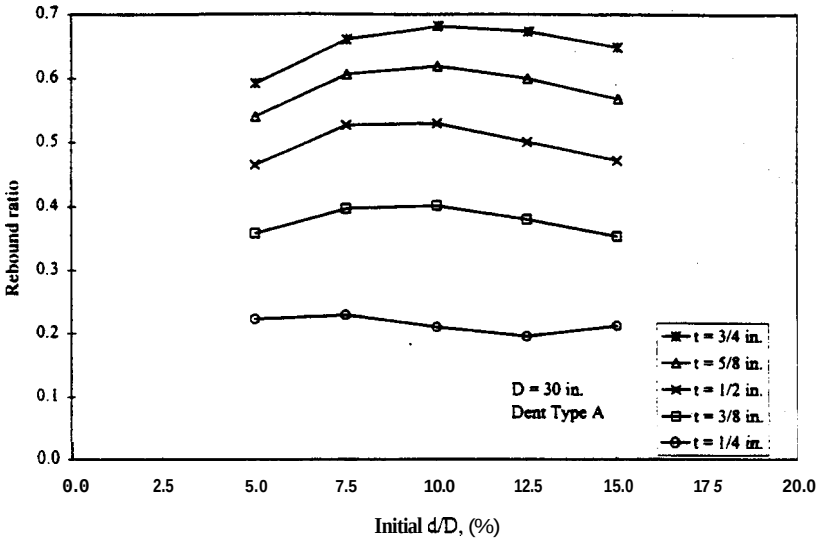

Figure 4-31: Rebound Ratio **vs.** initial **dent depth** (*d/D*) **for** all Type **A dents in 30 in. pipes.**

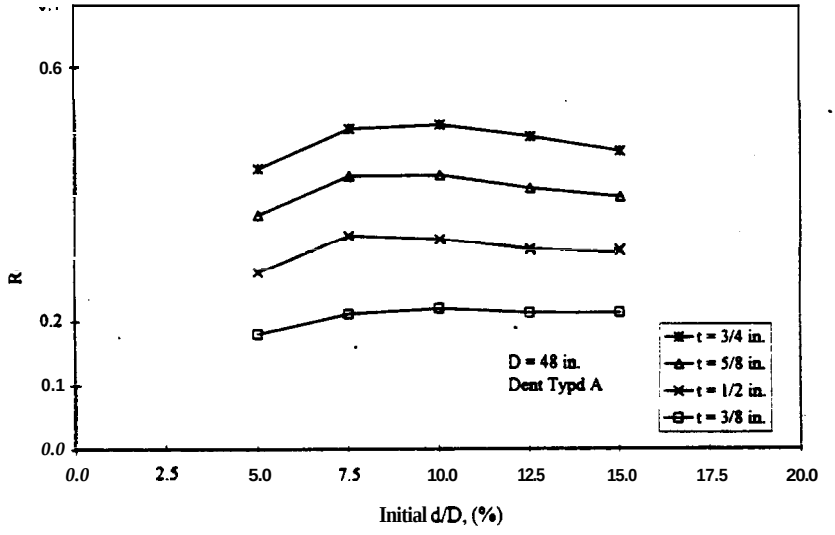

Figure 4-32: Rebound Ratio vs. initial **dent depth** (*d/D*) **for** all Type **A dents in 48 in. pipes.**

The Rebound Ratios for a specific pipe were averaged to yield an approximate value applicable to all dent depths. Rebound Ratio data for all pipe sizes for dent Type A is given in Table 4-7. Models with diameters of 24 in. or less used a pipe grade of X60 (60 ksi). Models with larger diameters used a pipe grade B (35 ksi). An increase in pipe grade allows an increase in design pressure. An increase in pressure causes an increase in dent rebound. Thus, the pipes modeled at grade X60 would experience more rebound than similar pipes modeled with grade B. The Rebound Ratio values in Table 4-7 are shown in Fig. 4-33. The discontinuity in the graph between the 24 in. and 30 in. diameters is due to the change in pipe grades modeled.

Table 4-7. Rebound ratios for Type A dents.

Thickness, t (in.)	Diameter, D (in.)					
	Grade 60X			Grade B		
	12	18	24	30	36	48
0.250	0.34	0.25	0.20	0.21	0.17	-----
0.375	0.44	0.35	0.29	0.40	0.33	0.22
0.500	0.54	0.45	0.39	0.53	0.46	0.33
0.625	-----	-----	0.50	0.62	0.56	0.43
0.750	----	--	----	0.68	0.63	0.51

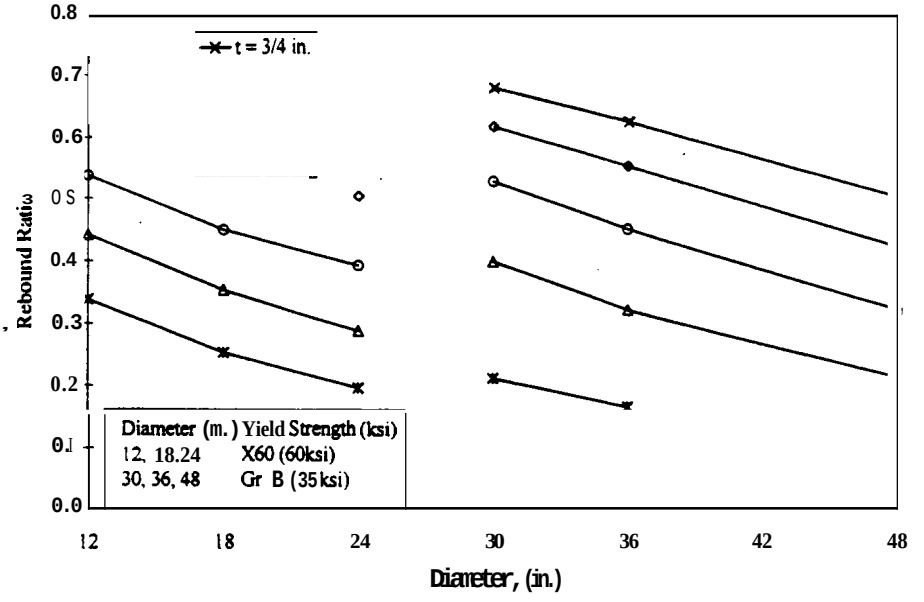

Figure 4-33: Rebound Ratio for **Type** A dents.

4.4.4 Dent Type BH Rebound Behavior

All Type BH dents have a similar rebound behavior. The short dent length causes the dent to maintain its shape thru indenter removal and pressurization unlike longer dents which are susceptible to bulging as discussed with **Type A** and longer dent types. The general rebound behavior is shown for Pipe 18-3. Figure 4-34 shows the shape of Type BH dents at indentation prior to removal of the indenting force. The initial rebound shape is given in Fig. 4-35. The final rebound shape is given in Fig. 4-36. The contact region remains at an equal depth fiom indentation through initial and final rebound. Thus, the location of maximum dent depth is always at the center of the dent unlike **Type A** dents.

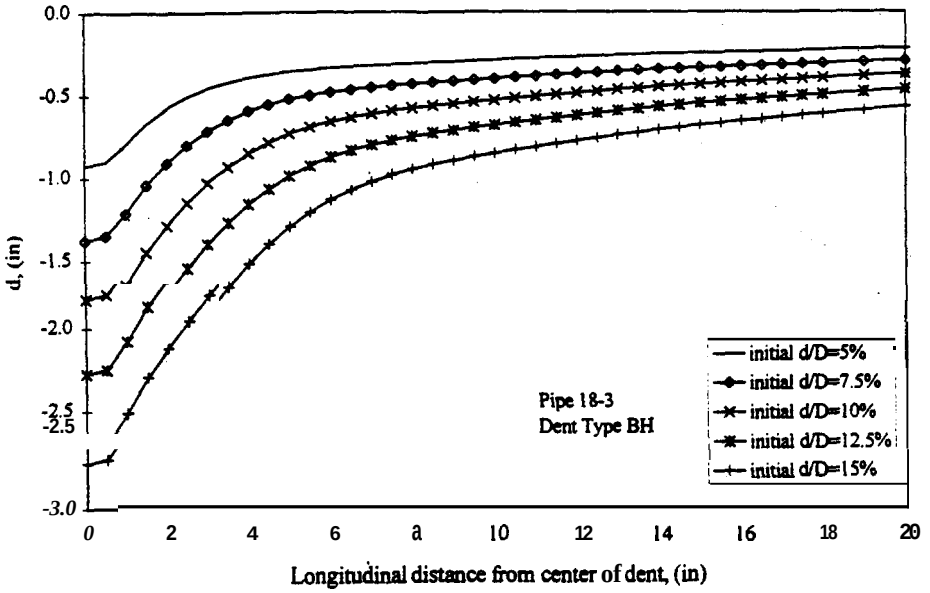

Figure 4-34: Type BH dent depth indentation for Pipe **18-3.**

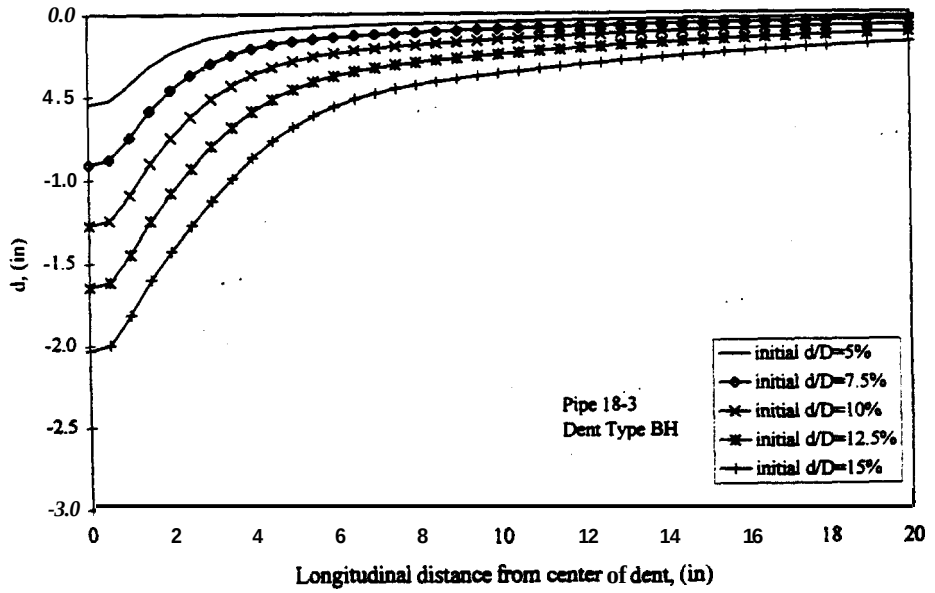

Figure 4-35: Type BH dent depth after **initial** rebound **for Pipe 18-3.**

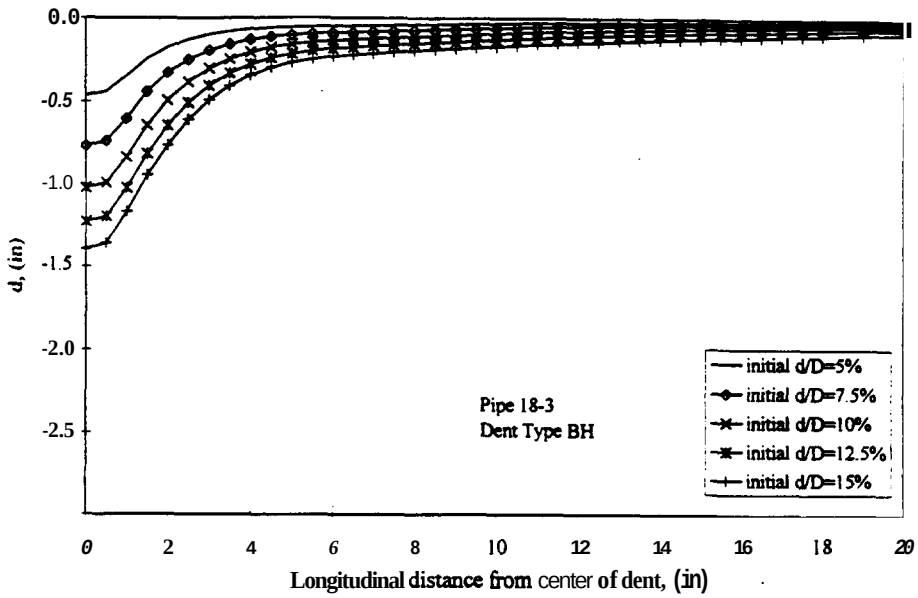

Figure 4-36: Type BH dent depth after final rebound for Pipe 18-3.

Possible locations of fatigue failure are not easily predictable for Type BH dents based strictly on the rebound behavior. The short dent length creates a sharp profile with high dent stiffness when compared to longer dents. Fatigue failures are not expected in the dent contact region due to the high compressive residual stress from indentation. Failure locations develop in the periphery of the dent contact region where no contact damage exists. This failure location is not obvious without prior knowledge of fatigue behavior of short dents. Bulging behavior was not noticed for any of the pipe sizes modeled. Thus, all Type BH dents in all pipe sizes will behave as short dents.

Type BH dents have less rebound when compared to Type A dents. The pipe parameters influence rebound of Type BH dents similarly to how they influenced rebound of Type A dents. The relationship of initial and final depths found for Type A dents also apply to Type BH dents. Graphs of final dent depth (d/D) vs. initial dent depth (d/D) are given for the 12 in., 30 in., and 48 in. diameter pipes in Figs. 4-37, 4-38, and 4-39, respectively. For each thickness, the linear relationship of initial and final dent depths found for Type A dents also applies for Type BH

dents. The data series all have Y intercepts near the origin. Thus, the constant Rebound Ratio is applicable to Type BH dents of different depth for a given pipe. Figures 440, 441, and 4-42 give graphs of Rebound Ratio vs. initial dent depth for 12 in., 30 in., and 48 in. diameter pipes, respectively. As with the Type A dents, the Rebound Ratio remains constant with respect to dent depth for a given pipe.

The Rebound Ratios for a specific pipe were averaged to get the approximate value for all dent depths. Rebound Ratio data for all pipe sizes for dent Type BH is given in Table 4-8. The averaged Rebound Ratios are displayed graphically in Fig. 4-43. As discussed with the Type A Rebound Ratios, the discontinuity between the 24 in. and 30 in. diameters represent a change in pipe grade.

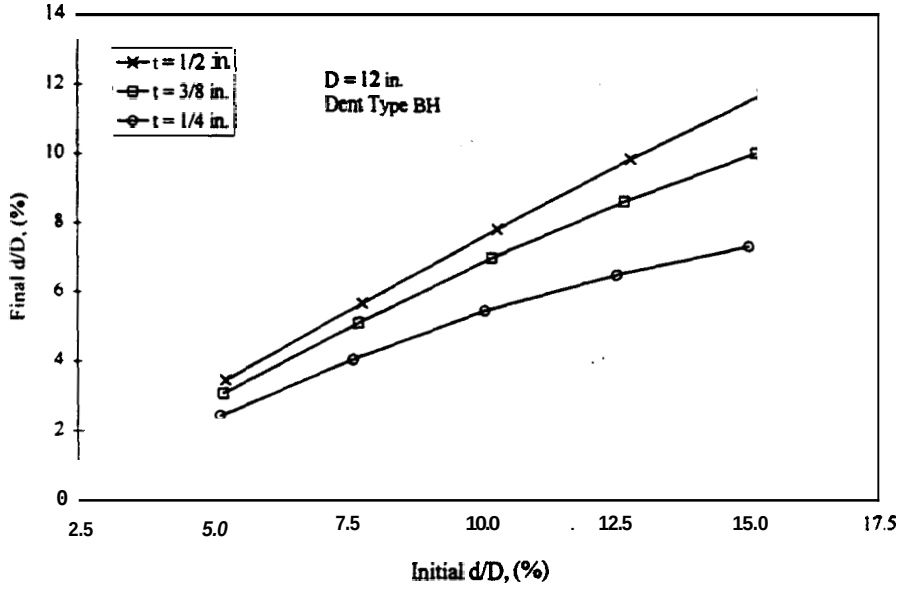

Figure 4-37: Final dent depth (d/D) vs. initial dent depth (d/D) for all Type BH dents in 12 in. pipes.

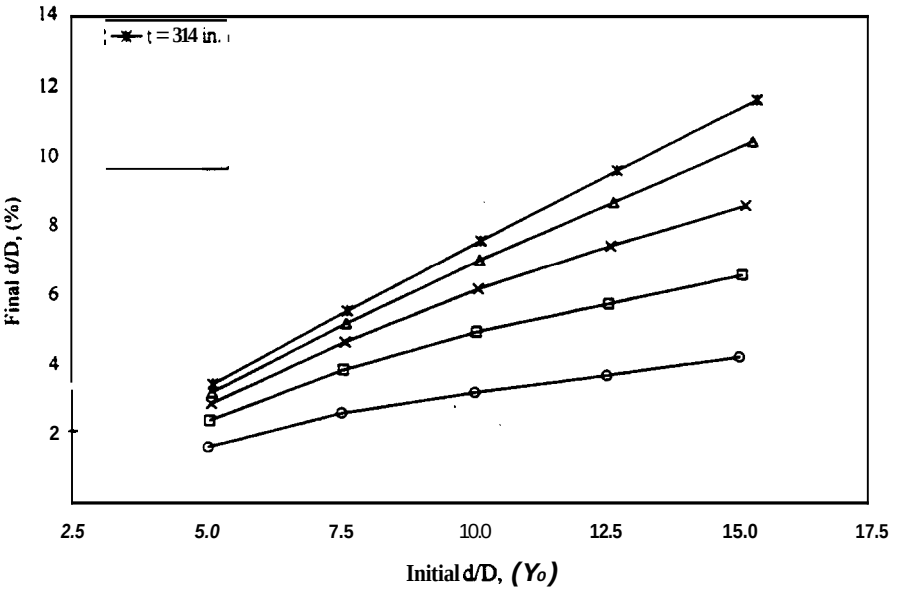

Figure 4-38: Final dent depth (*d/D*) vs. initial dent depth (*d/D*) for all Type BH dents in 30 in. pipes.

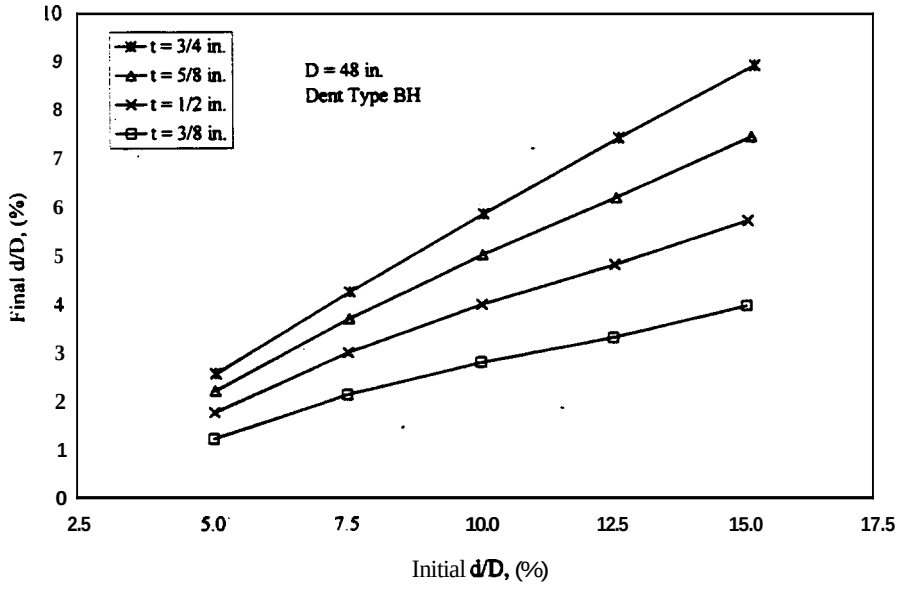

Figure 4-39: Final dent depth (*d/D*) vs. initial dent depth (*d/D*) for all Type BH dents in 48 in. pipes.

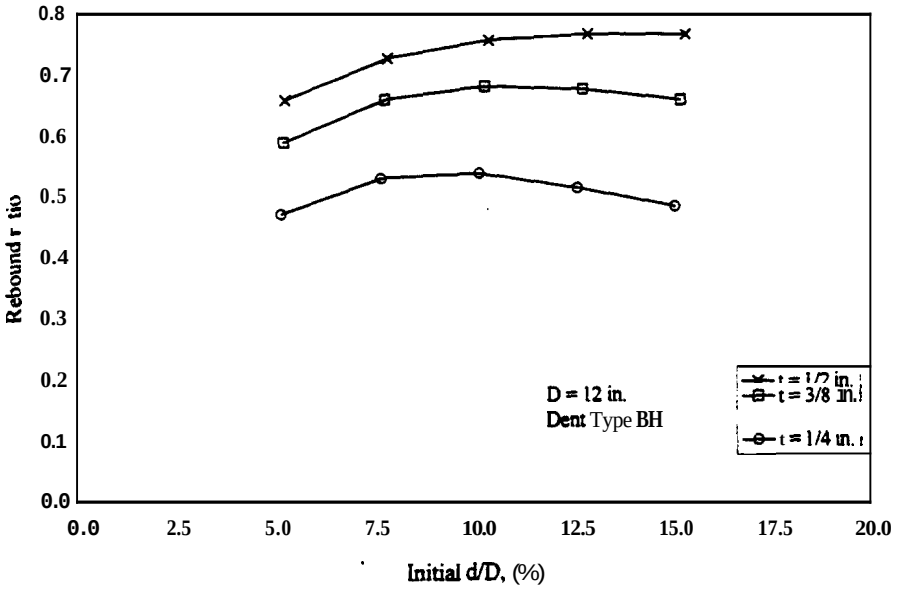

Figure 4-40: Rebound Ratio **vs. initial dent depth for all** Type **BH dents in 12 in. pipes.**

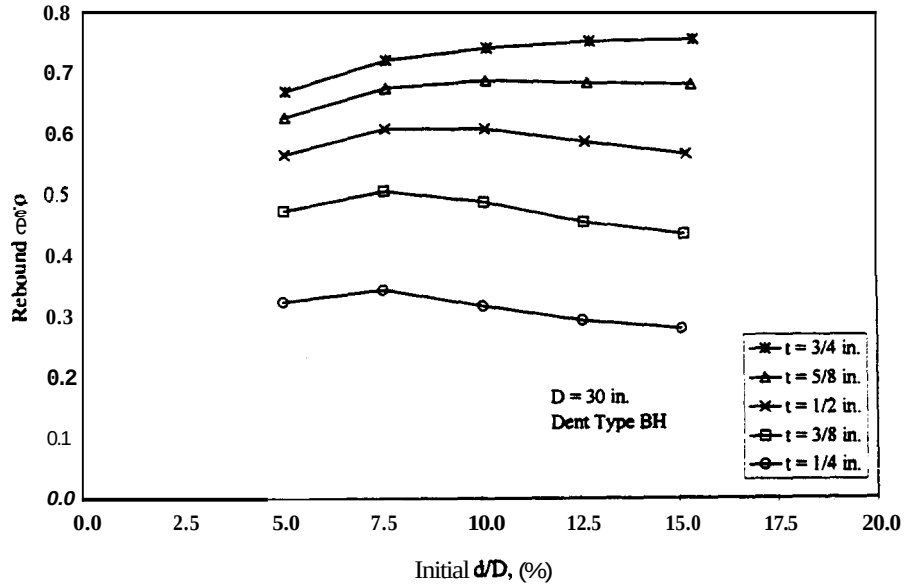

Figure 4-41: Rebound Ratio vs. initial **dent depth for all** Type **BH dents in 30 in. pipes.**

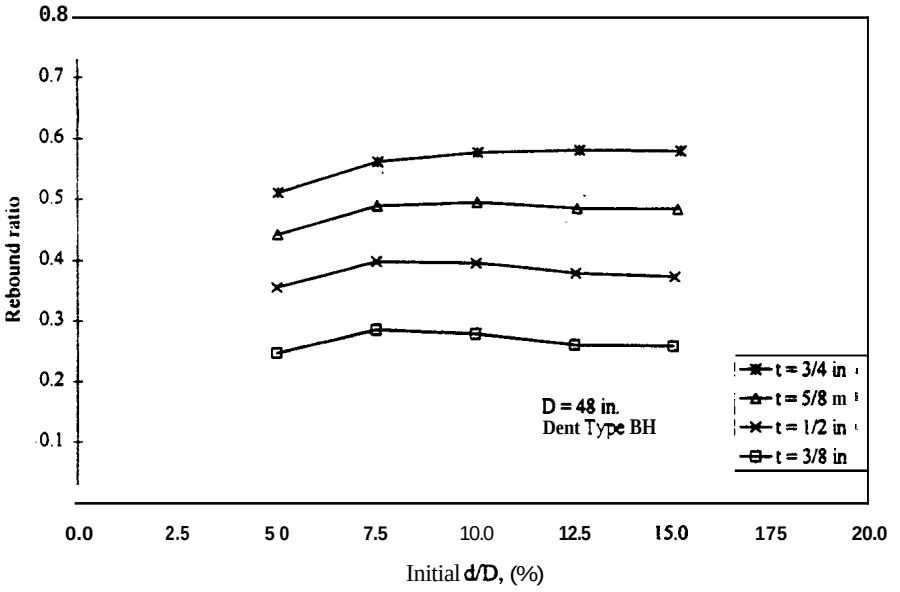

Figure 4-42: Rebound Ratio vs. initial **dent depth for all** Type **B H dents in 48 in. pipes.**

Table 4-8: Rebound Ratios for Type **B H dents.**

Thickness, t (in.)	Diameter, D (in.)					
	Grade 60X			Grade B		
	12	18	24	30	36	48
0.250	0.54	0.40	0.31	0.32	0.25	-----
0.375	0.68	0.56	0.46	0.49	0.41	0.28'
0.500	0.76	0.66	0.58	0.61	0.54	0.40
0.625	-----	-----	0.65	0.69	0.63	0.50
0.750	-----	-----	----	0.74	0.69	0.58

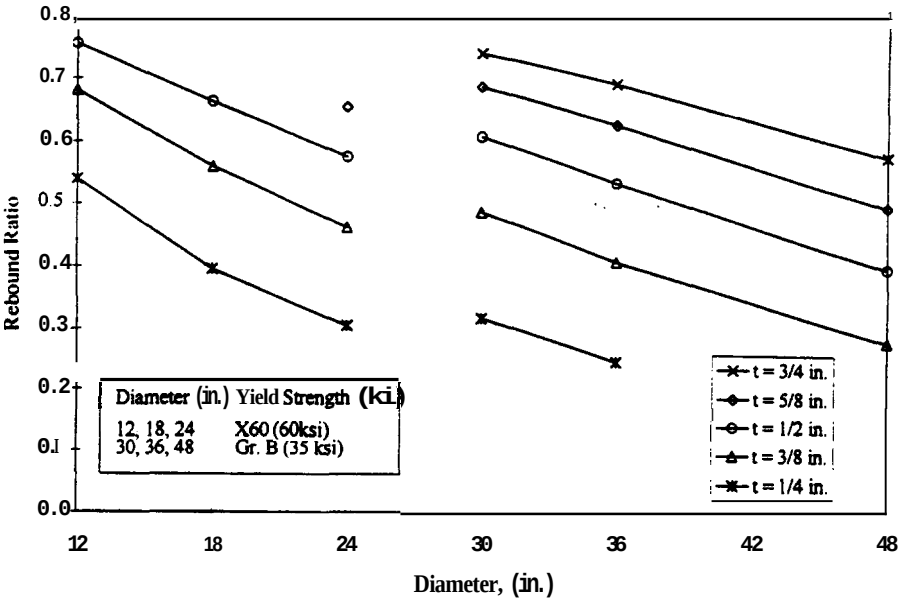

Figure 4-43: Rebound Ratio of Type BH dents.

4.4.5 Dent Type G Rebound Behavior

Type G dents exhibit long dent behavior. The length of the Type G indenter is twice the length of the Type A indenter (12 in. versus 6 in.). Type G dents develop the bulging rebound behavior of the indenter contact region as in Type A dents. The rebound behavior is shown for Pipe 18-3. Figure 4-44 shows the shape of Type G dents at indentation. The dent shape after initial and final rebound is given in Figs. 4-45 and 4-46. As found with Type A dents, the bulging behavior causes the final depths at the center of the dent to have similar values for dents of different initial depth. Thus, dent depth measurements will be recorded at the edge of the contact region where the maximum depth occurs. The length of the bulged region is greater for Type G dents when compared to Type A dents due to the increase in indenter length. The increase in length causes a reduction in curvature in the longitudinal direction of the bulge as compared to Type A dents. This corresponds to an increase in the dent flexibility when compared to dents with shorter lengths.

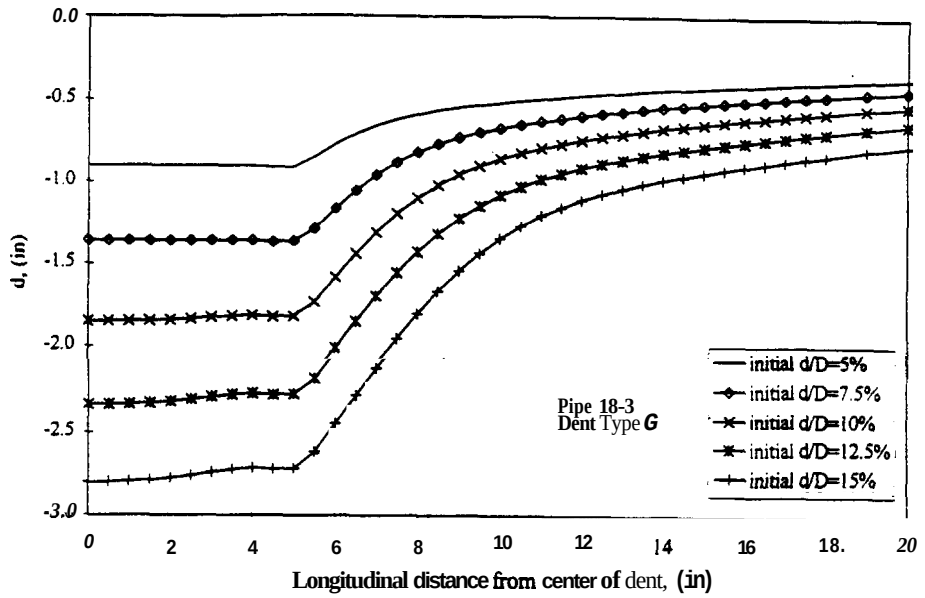

Figure 4-44: Type G dent at indentation for Pipe 18-3.

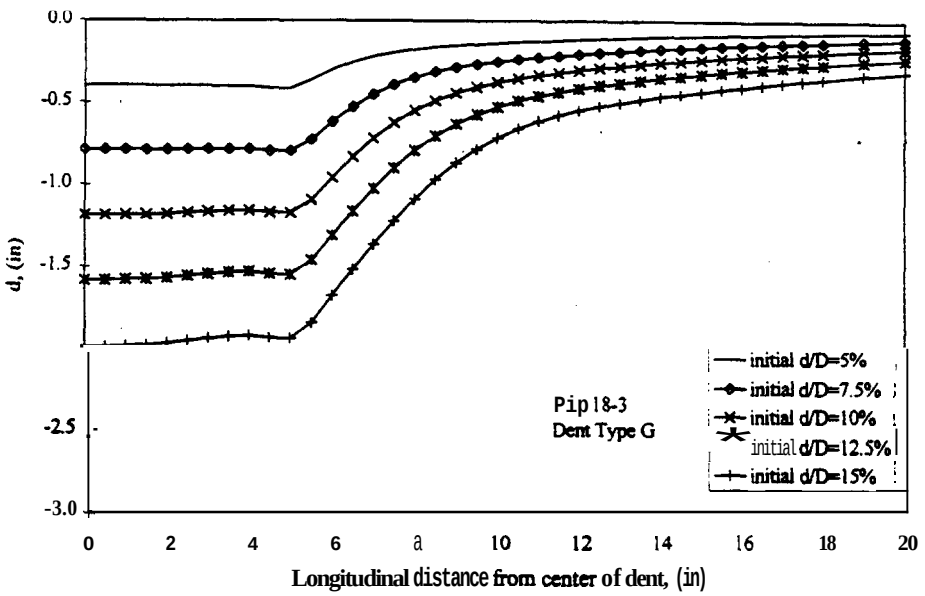

Figure 4-45: Type G dent after initial rebound for Pipe 18-3.

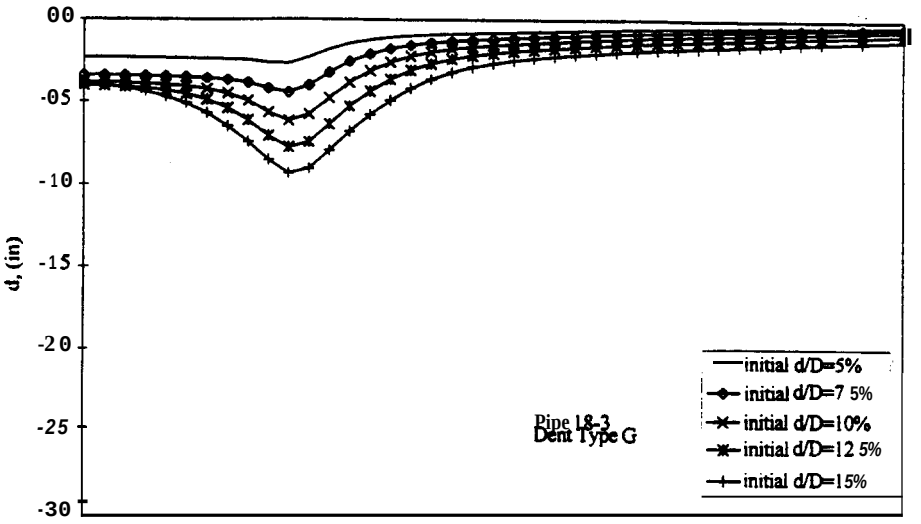

Figure 4-46: Type G dent depth after final rebound for Pipe 18-3.

Type G dents in larger diameter pipes are more likely to have the bulging behavior *than* Type A dents. The dent shape after final rebound for Type G dents in Pipe 30-4 is given in Fig. 4-47. The dents all have the bulging rebound behavior. Type A dents in Pipe 30-4 did not develop the bulging behavior (Fig. 4-26). The comparison between Type A and G dents for Pipe 30-4 show how dent length influences the rebound behavior of dents. Type G dents do not have bulging rebound behavior only in thick large diameter pipes. For example, the dent shape after final rebound for Type G dents in Pipe 48-6 is given in Fig. 4-48. The shallower depths have slight bulging behavior of the contact region. The deeper dents do not develop bulges due to the increase in dent stiffness from increased dent depth.

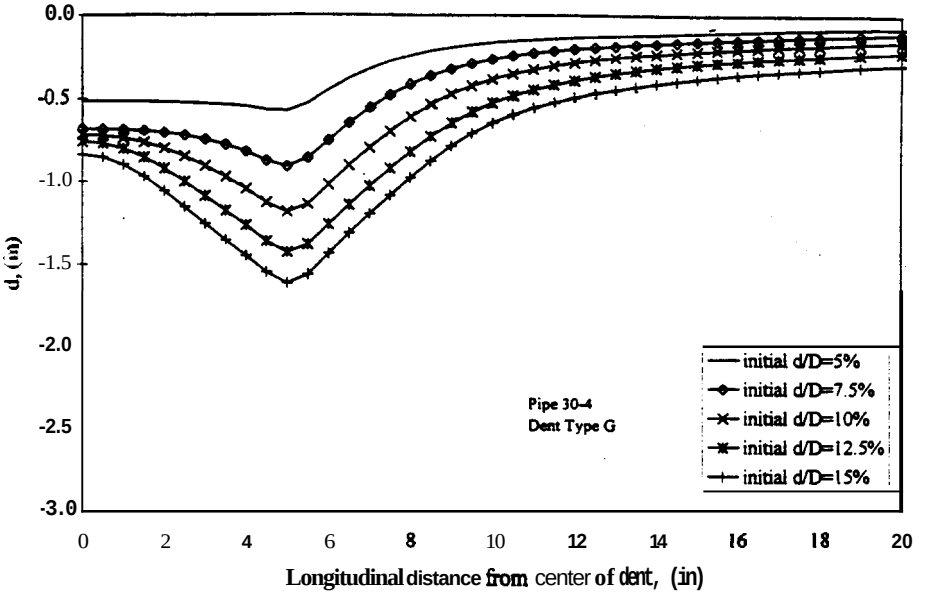

Figure 4-47: Type *G* dent depth after final rebound for Pipe 30-4.

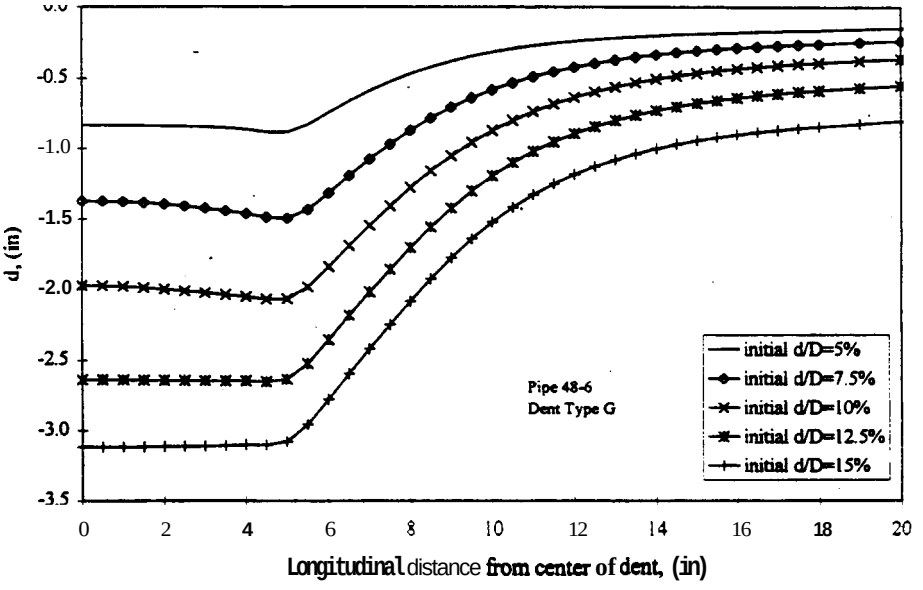

Figure 4-48: Type *G* dent depth after final rebound for Pipe 48-6.

The relationship of initial and final dent depths of Type G dents has the same correlation as Type A and Type BH dents. Graphs of final dent depth (d/D) vs. initial dent depth (d/D) are given for the 12 in., 30 in., and 48 in. diameter pipes in Figs. 4-49, 4-50, and 4-51, respectively. For each thickness, the linear relationship of initial and final depths exists for Type G dents. Figures 4-52, 4-53, and 4-54 give graphs of Rebound Ratio vs. initial dent depth for 12, 30, and 48 in. diameter pipes, respectively. As with the other dent types, the Rebound Ratio remains constant with respect to dent depth for a given pipe.

The Rebound Ratios for a specific pipe were averaged to get the approximate value for all dent depths. Rebound Ratio data for all pipe sizes for dent Type G is given in Table 4-9. The averaged Rebound Ratios are displayed graphically in Fig. 4-55. As discussed with the Type A Rebound Ratios, the discontinuity between the 24 in. and 30 in. diameters represents a change in pipe grade.

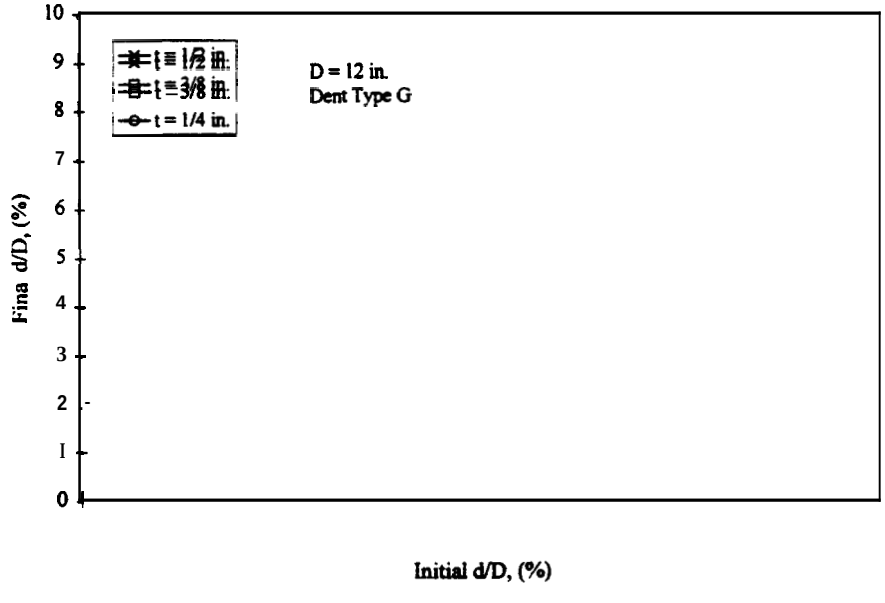

Figure 4-49: Final dent depth (d/D) vs. initial dent depth (d/D) for all Type G dents in 12 in. pipes.

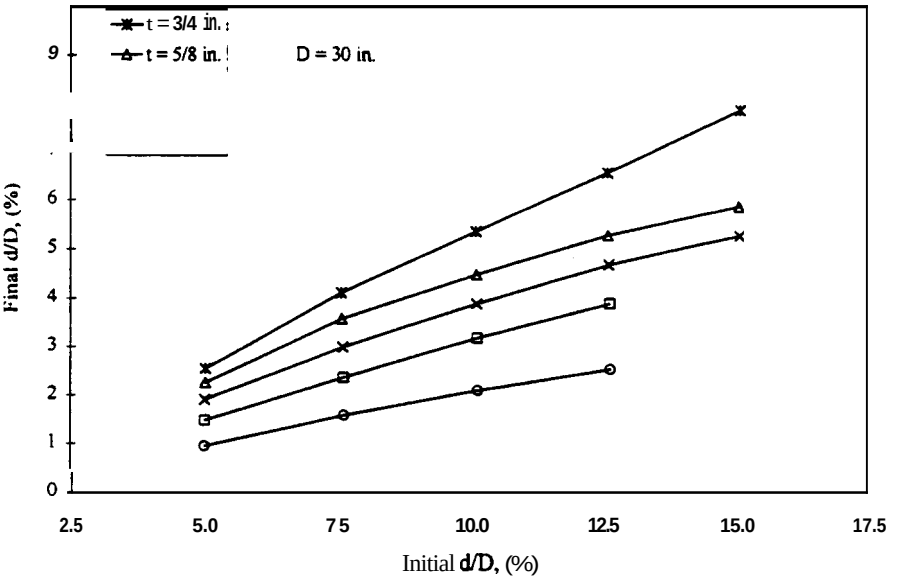

Figure 4-50: Final **dent depth** (d/D) **vs. initial dent depth** (d/D) **for all Type G dents in 30 in. pipes.**

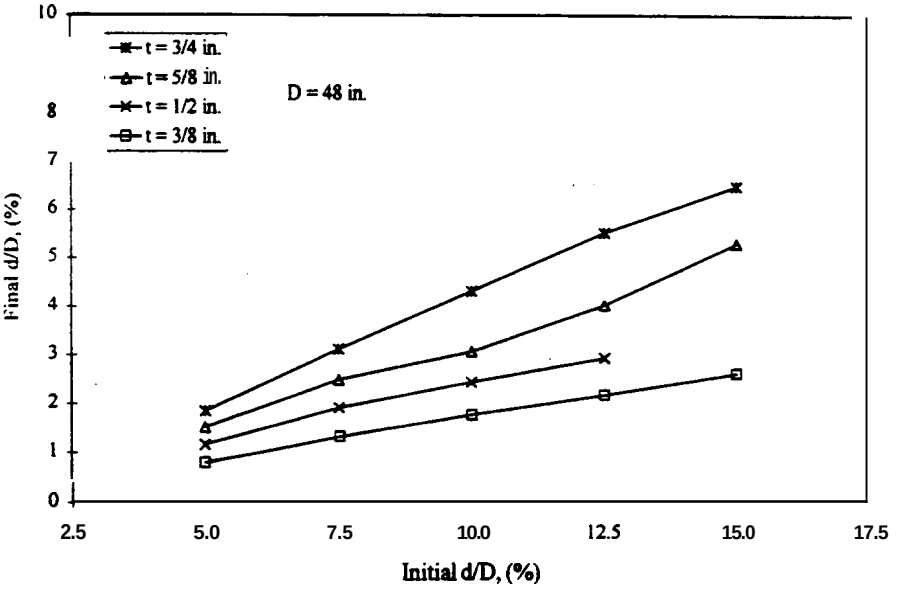

Figure 4-51: Final **dent depth** (d/D) **vs.** initial **dent depth** (d/D) **for** all **Type G dents in 48 in. pipes.**